Mon. Not. R. Astron. Soc. **000**, 1–?? (2002) Printed 7 May 2014 (MN LATEX style file v2.2)

STEP: The VST survey of the SMC and the Magellanic Bridge. I. Overview and first results.⋆

V. Ripepi,[1]† M. Cignoni,[2,3] M. Tosi,[3] M. Marconi,[1] I. Musella,[1] A. Grado,[1]
L. Limatola,[1] G. Clementini,[3] E. Brocato,[4] M. Cantiello,[5] M. Capaccioli,[6]
E. Cappellaro,[7] M-R. L. Cioni,[8,9] F. Cusano,[3] M. Dall'Ora,[1] J. S. Gallagher III,[10]
E. K. Grebel,[11] A. Nota,[2,12] F. Palla,[13]D. Romano,[3] G. Raimondo,[5]
E. Sabbi,[2] F. Getman,[1] N. R. Napolitano,[1] P. Schipani,[1] S. Zaggia[7]

[1] *INAF-Osservatorio Astronomico di Capodimonte, Via Moiariello 16, 80131, Naples, Italy*
[2] *Space Telescope Science Institute, 3700 San Martin Drive, Baltimore, USA*
[3] *INAF-Osservatorio Astronomico di Bologna, via Ranzani 1, Bologna, Italy*
[4] *INAF-Osservatorio Astronomico di Roma, Via Frascati 33, 00040, Monte Porzio Catone (RM), Italy*
[5] *INAF-Osservatorio Astronomico di Teramo, Via M. Maggini, 64100 Teramo, Italy*
[6] *Dipartimento di Fisica, Università "Federico II", Naples, Italy*
[7] *INAF-Osservatorio Astronomico di Padova, Vicolo dell'Osservatorio 5, 35122 Padova, Italy*
[8] *University of Hertfordshire, Physics Astronomy and Mathematics, Hatfield AL10 9AB, UK*
[9] *Leibnitz-Institut für Astrophysik Potsdam, An der Sternwarte 16, 14482 Potsdam, Germany*
[10] *Department of Astronomy, University of Wisconsin-Madison, 5534 Sterling, 475 North Charter Street, Madison, WI 53706, USA*
[11] *Astronomisches Rechen-Institut, Zentrum für Astronomie der Universität Heidelberg, Mönchhofstr 12-14, D-69120 Heidelberg, Germany*
[12] *European Space Agency, Research and Scientific Support Department, Baltimore, MD, USA*
[13] *INAF-Osservatorio Astrosico di Arcetri, Largo E. Fermi 5, 50125 Firenze, Italy*

ABSTRACT

STEP (the **S**MC in **T**ime: **E**volution of a **P**rototype interacting late-type dwarf galaxy) is a Guaranteed Time Observation survey being performed at the VST (the ESO VLT Survey Telescope). STEP will image an area of 74 deg^2 covering the main body of the Small Magellanic Cloud (32 deg^2), the Bridge that connects it to the Large Magellanic Cloud (30 deg^2) and a small part of the Magellanic Stream (2 deg^2). Our g, r, i, H_α photometry is able to resolve individual stars down to magnitudes well below the main-sequence turnoff of the oldest populations. In this first paper we describe the observing strategy, the photometric techniques, and the upcoming data products of the survey. We also present preliminary results for the first two fields for which data acquisition is completed, including some detailed analysis of the two stellar clusters IC 1624 and NGC 419.

Key words: galaxies: Magellanic Clouds – galaxies: photometry – stars: Hertzsprung-Russell and colour-magnitude diagrams – galaxies: distances and redshifts – galaxies: star formation – galaxies: stellar content – galaxies: star clusters: general – surveys

1 INTRODUCTION

Dwarf galaxies in the Local Group provide a distinct laboratory for studying and testing galaxy formation theories and cosmology. To understand the history of formation and evolution of galaxies, as well as their interactions with the environment, we need to study the 3D structure and the distributions of age, chemical abundance and kinematics of both stellar and gaseous components. We also need to obtain a global picture of the star formation history (SFH), accounting for both the intrinsic evolution and the effects of interactions with neighbouring systems. This is best achieved in nearby galaxies, where individual stars can be resolved down to faint absolute magnitudes, thus probing stellar

⋆ This work is based on INAF-VST guaranteed observing time under ESO programmes 089.D-0258; 090.D-0172

† E-mail: ripepi@oacn.inaf.it

masses from high to low and ages from young to old. In closer systems, the stellar populations can be characterised in exquisite detail, with deep photometry and spectroscopy, and their SFHs can be reliably derived over the whole Hubble time, from the most recent epochs back to the earliest ones (see e.g., Tolstoy et al. 2009, and references therein).

The Small Magellanic Cloud (SMC, $M_V = -16.8 \pm 0.2$ mag; $D_\odot \sim 64$ Kpc; de Vaucouleurs et al. 1991; Udalski et al. 1999) is the closest dwarf galaxy of late morphological type, hence the ideal target for detailed studies of the properties of this most common class of galaxies. Its mass (between 1 and 5 $\times 10^9$ $M_\odot$, e.g., Kallivayalil et al. 2006; Bekki & Stanimirović 2009, and references therein) is at the upper limit of the typical late-type dwarf masses. Its high gas content ($M_{HI} = 4 \times 10^8$ $M_\odot$ Brüns et al. 2005) and low present-day metallicity (Z=0.004, see e.g., Russell & Bessell 1989) are also common features of dwarf irregulars (dIrr) and starburst dwarfs.

The old populations in dIrrs may be representative of the stellar content of the early, gas–rich galaxies that are believed to have contributed significantly to the build-up of more massive galaxies (e.g., De Lucia & Helmi 2008; Cooper et al. 2010) more than 9 Gyr ago. These old stellar populations are quite a bit more metal-poor than the comparatively high present-day SMC metallicity of Z=0.004 (see e.g., Kunth & Östlin 2000).

As a member of the nearest group of interacting galaxies, the SMC is also an ideal benchmark to study the effects of tidal interactions on galaxy evolution. In fact there are clear signatures that the SMC is interacting with its neighbours, the Large Magellanic Cloud (LMC) and the Milky Way (MW). In particular, the Magellanic Clouds (MCs) are connected by an HI-dominated gaseous Bridge (Hindman, Kerr, & McGee 1963; Irwin, Kunkel, & Demers 1985; Harris 2007) that, like the Magellanic Stream, may result from their mutual gravitational effects and/or the influence of the MW. The SMC Wing, the portion of the SMC main body protruding asymmetrically towards the LMC (Shapley 1940), may also be the result of tidal forces. Also, the bar of the SMC, which stands out when using young populations as tracers, has a highly asymmetric and elongated structure with its north–eastern part closer to us than its south–western part (Haschke, Grebel, & Duffau 2012). To complicate matters further, remarkable line-of-sight depth variations are well established in the SMC. For instance, Hatzidimitriou & Hawkins (1989), using horizontal branch (HB) and red clump (RC) stars, found that the northeastern periphery of the galaxy (at more than 2 kpc from the optical centre) suffers an average depth of 17 kpc with a maximum of 23 kpc, while the southwest region shows a depth of about 10 kpc on average. More recently, Subramanian & Subramaniam (2009) found a depth between 0.67 kpc and 9.53 kpc, with an increase near the optical centre. Finally, Glatt et al. (2008b) found depths between 10 and 17 kpc using the RC of several populous star clusters.

State-of-the-art computations based on Hubble Space Telescope (HST) data (Kallivayalil et al. 2013) assume that the Clouds are bound to each other, with the SMC on an elliptical orbit around the LMC. It was estimated that the frequency of MC-like systems in the Universe is only a few percent (e.g., Robotham et al. 2012) and they may have entered the MW potential only recently.

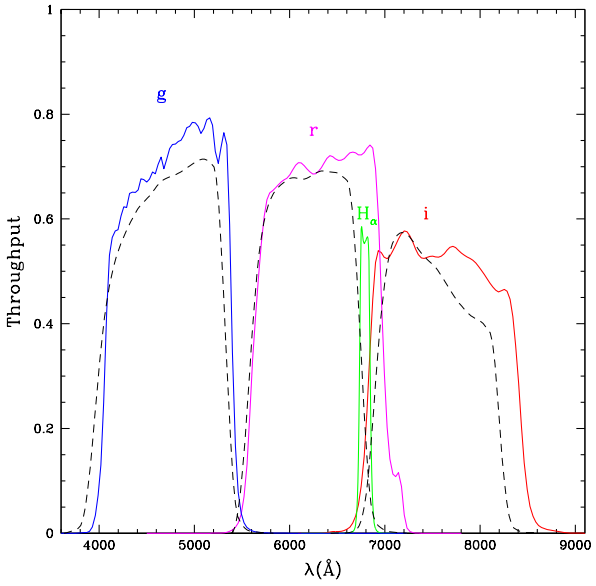

Figure 1. Transmittance of the filters used in STEP (solid lines). The contribution of the CCD is included. The dashed curves represent the transmission curves for the corresponding SDSS filters (properly rescaled to favour the comparison).

The Bridge holds important clues about the most recent (the last ∼100 Myr) interaction between the Clouds, its own formation history and possible origin. Intermediate-age and old stars, probably stripped by either Cloud, may also be present in the Bridge (Bagheri et al. 2013; Noël et al. 2013) and would provide additional information about its origin.

A wealth of data on the SMC are available in the literature, although not as complete as for its bigger companion, the LMC. Yet, we are still missing crucial information for our understanding of how the SMC has formed and evolved. For these reasons, a long-term international project has been set up with the aim of studying in detail the stellar populations, the structure and the evolution of the SMC in space and time, thanks to the exploitation of high performance telescopes, such as the HST, the VLT (Very Large Telescope) and other 10 m class telescopes. The project aims at collecting both photometric and spectroscopic data to study the (variable and non-variable) stellar populations of the SMC, from the oldest to the youngest objects and derive their chemical abundances, spatial distribution and kinematics. In particular, HST is providing high spatial resolution photometry of selected SMC fields, along with old and young clusters (P.I.s J. Gallagher and A. Nota, see e.g., Nota et al. 2006; Sabbi et al. 2007; Glatt et al. 2008a,b, 2009, 2011; Sabbi et al. 2009; Cignoni et al. 2010, 2011, 2012, 2013), whereas VLT spectroscopy with FORS in the CaII triplet

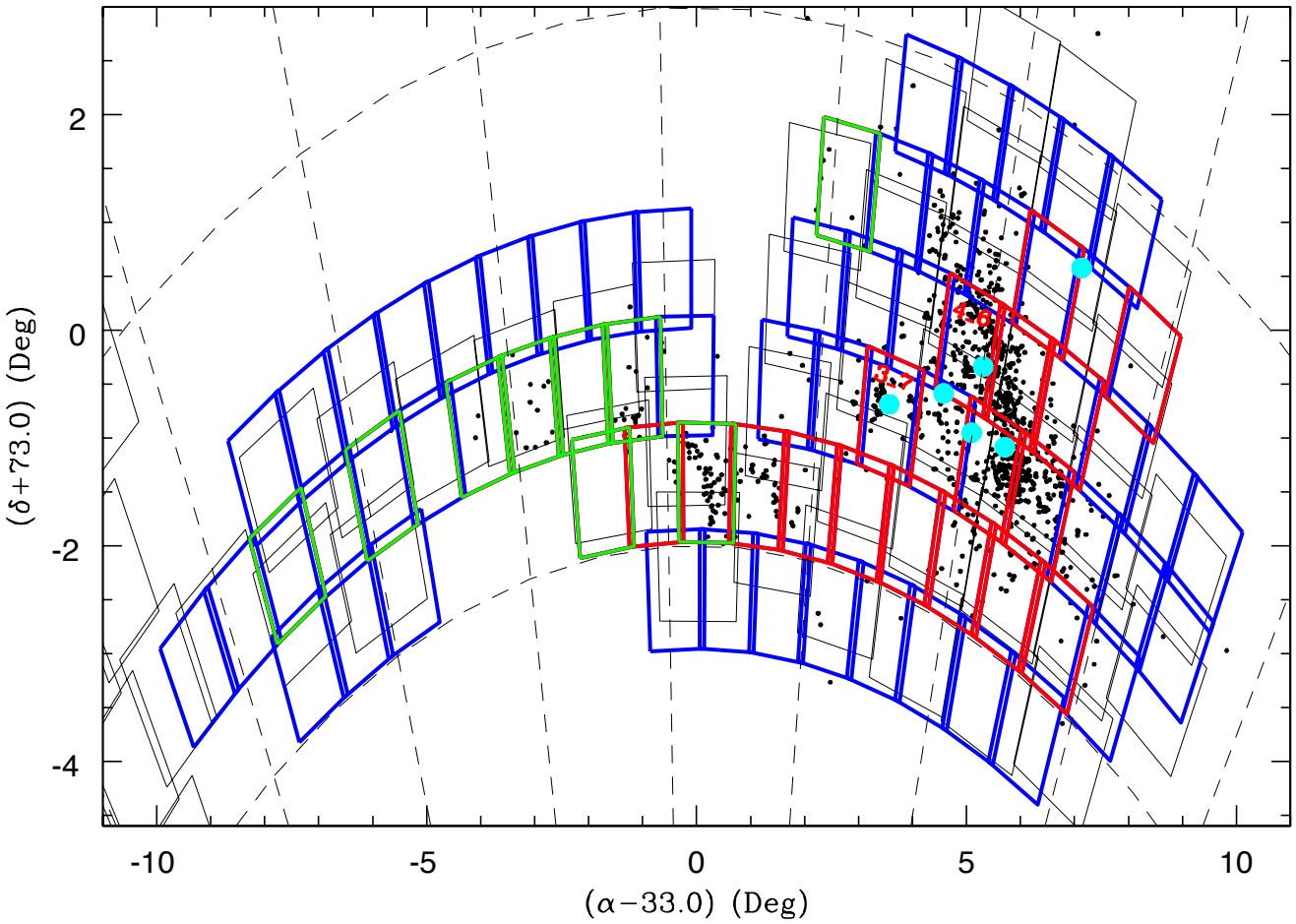

Figure 2. Map of STEP's tiles (the two tiles centred in the direction of the Magellanic Stream are out of the figure). To highlight the location of the SMC body and of part of the Bridge, black dots indicate the position of known star clusters and associations (according to Bica et al. 2008). The thick boxes correspond to the 1 deg^2 FoV of the VST tiles. Red boxes represent tiles whose observations are completed, green boxes those with completed time-series photometry, and blue boxes the remaining ones. To find a correspondance with Tab. 2, note that the tiles from south to north are those with prefix "1_" and "6_", respectively. From west to east the first and last tiles have suffix "_1" and "_21", respectively. For comparison, grey thin boxes show the VMC tiles, whereas the HST fields described by Sabbi et al. (2009) are the small cyan filled circles (note that the true size of HST fields is significantly smaller). The two tiles analysed in this work (tiles 3_7 and 4_6) are labelled.

(P.I. E. Grebel) allows to study the age-metallicity relation of the SMC clusters (Kayser et al. 2008).

In this context, the scope of this paper is to present the first results from the VST (VLT Survey Telescope) survey STEP (The **S**MC in **T**ime: **E**volution of a **P**rototype interacting late-type dwarf galaxy, PI V. Ripepi). We describe the STEP survey in detail in Section 2, while the data reduction is reported in Section 3. The resulting CMDs for two fields are discussed in Section 4, an example of analysis of star clusters is given in Section 5. A brief summary closes the paper.

2 THE STEP SURVEY

The STEP survey is based on VST Guaranteed Time Observations (GTO; PI V.Ripepi). The survey aims at performing the first deep and homogeneous optical photometric monitoring of the entire SMC body as well as of the Bridge. The VST (Capaccioli & Schipani 2011) is an ideal instrument for a homogeneous survey of the properties of the stellar populations present in the SMC components (main body, Wing, Bridge, outskirts), thanks to its wide Field–of–View (FoV, 1 deg^2) and a magnitude limit optimal for the SMC distance. It provides the most natural complement to HST imaging, which reaches much fainter magnitudes with high spatial resolution, but over very small fields of view.

Some of us (V. Ripepi, M.R. Cioni., G. Clementini and M. Marconi) are deeply involved in the VMC@VISTA European Southern Observatory (ESO) Public survey (P.I: M.R. Cioni) that is achieving $YJK_{\rm s}$ photometry of the Magellanic System (LMC, SMC, Bridge, Stream, 184 deg^2 at Ks=20.3 mag). STEP and VMC@VISTA are designed to complement each other: the target fields of the two surveys overlap com-

Table 2. STEP field centres and status of observations as of 2014, January. A "TS" in the columns "MODE" means that the field was observed in time-series mode. In the "NOTES" columns: C=Completed; S=Started. The two planned tiles in the direction of the Magellanic Stream are not included here as their centres coincides with those reported in Tab. A.4 of Cioni et al. (2011).

Field	RA (J2000)	DEC (J2000)	MODE	NOTES	Field	RA (J2000)	DEC (J2000)	MODE	NOTES
1_3	00:32:11.376	-75:24:00.360			3_16	03:21:58.800	-73:24:58.680		S
1_4	00:47:17.760	-75:24:00.360			3_17	03:35:22.584	-73:24:58.680	TS	C
1_5	01:02:24.120	-75:24:00.360			3_18	03:48:46.368	-73:24:58.680		S
1_6	01:17:30.504	-75:24:00.360			3_19	04:02:10.152	-73:24:58.680	TS	C
1_7	01:32:36.888	-75:24:00.360			3_20	04:15:33.960	-73:24:58.680		
1_8	01:47:43.272	-75:24:00.360			3_21	04:28:57.744	-73:24:58.680		
1_9	02:02:49.632	-75:24:00.360			4_1	00:00:38.544	-72:25:27.480		
1_10	02:17:56.016	-75:24:00.360			4_2	00:13:19.584	-72:25:27.480		
2_2	00:15:40.368	-74:24:29.520			4_3	00:26:00.648	-72:25:27.480		S
2_3	00:29:52.224	-74:24:29.520		C	4_4	00:38:41.712	-72:25:27.480		C
2_4	00:44:04.104	-74:24:29.520		C	4_5	00:51:22.752	-72:25:27.480		C
2_5	00:58:15.984	-74:24:29.520		C	4_6	01:04:03.816	-72:25:27.480		C
2_6	01:12:27.864	-74:24:29.520		S	4_7	01:16:44.856	-72:25:27.480		S
2_7	01:26:39.744	-74:24:29.520		C	4_8	01:29:25.920	-72:25:27.480		
2_8	01:40:51.624	-74:24:29.520		C	4_9	01:42:06.960	-72:25:27.480		S
2_9	01:55:03.504	-74:24:29.520		C	4_12	02:20:10.128	-72:25:27.480		
2_10	02:09:15.384	-74:24:29.520	TS	C	4_13	02:32:51.168	-72:25:27.480		
2_11	02:23:27.264	-74:24:29.520		C	4_14	02:45:32.232	-72:25:27.480		
2_12	02:37:39.120	-74:24:29.520		C	4_15	02:58:13.272	-72:25:27.480		
2_16	03:34:26.640	-74:24:29.520			4_16	03:10:54.336	-72:25:27.480		
2_17	03:48:38.520	-74:24:29.520			4_17	03:23:35.400	-72:25:27.480		
2_18	04:02:50.400	-74:24:29.520			4_18	03:36:16.440	-72:25:27.480		
3_1	00:01:01.992	-73:24:58.680			4_19	03:48:57.504	-72:25:27.480		
3_2	00:14:25.776	-73:24:58.680			4_20	04:01:38.544	-72:25:27.480		
3_3	00:27:49.560	-73:24:58.680			5_3	00:24:23.304	-71:25:56.640		C
3_4	00:41:13.368	-73:24:58.680		C	5_4	00:36:26.160	-71:25:56.640		S
3_5	00:54:37.152	-73:24:58.680		C	5_5	00:48:28.992	-71:25:56.640		C
3_6	01:08:00.936	-73:24:58.680		S	5_6	01:00:31.824	-71:25:56.640		
3_7	01:21:24.720	-73:24:58.680		C	5_7	01:12:34.680	-71:25:56.640		
3_8	01:34:48.504	-73:24:58.680			5_8	01:24:37.512	-71:25:56.640		
3_9	01:48:12.288	-73:24:58.680		S	5_9	01:36:40.344	-71:25:56.640	TS	C
3_11	02:14:59.856	-73:24:58.680			6_4	00:34:24.312	-70:26:25.440		
3_12	02:28:23.664	-73:24:58.680	TS	C	6_5	00:45:52.800	-70:26:25.440		S
3_13	02:41:47.448	-73:24:58.680	TS	C	6_6	00:57:21.264	-70:26:25.440		
3_14	02:55:11.232	-73:24:58.680	TS	C	6_7	01:08:49.752	-70:26:25.440		
3_15	03:08:35.016	-73:24:58.680	TS	C	6_8	01:20:18.216	-70:26:25.440		

Table 1. Characteristics of the filters used in the STEP survey.

Filter	$\lambda_{\rm mean}$ Å	$\lambda^a_{\rm eff}$ Å	$\lambda_{\rm min}$ Å	$\lambda_{\rm max}$ Å	$\Delta\lambda^b_{\rm eff}$ Å
g	4760	4680	3913	5573	1203
r	6326	6242	5405	7245	1314
i	7599	7509	6580	8741	1464
$H\alpha$	6789	6789	6675	6910	119

[a] central filter wavelength after the transmission curve was convolved with the spectrum of Vega

[b] effective filter width, equivalent to the horizontal size of a rectangle with height equal to the maximum transmission curve and with the same area of the one covered by the filter transmission curve

pletely in the SMC and Bridge region, and will provide, when completed, homogeneous $g, r, i, H_\alpha, Y, J, K_{\rm s}$ photometry for millions of stars in the SMC and the Bridge.

The colour magnitude diagram (CMD), containing stars born over the whole lifetime of the galaxy, is a fossil record of its SFH. With STEP we aim at investigating the stellar populations of the SMC with CMDs at least a couple of magnitudes fainter than the main sequence (MS) turn-off (MSTO) of the oldest population. This is crucial to break the age-metallicity degeneracy and safely recover the SFH of the investigated objects. The SFH will be derived using the synthetic CMD technique (e.g., Tosi et al. 1991; Cignoni & Tosi 2010). This kind of study has already been performed on several SMC fields both with ground-based and HST data (e.g., Dolphin et al. 2001; Zaritsky et al. 2002; Harris & Zaritsky 2004; McCumber et al. 2005; Chiosi et al. 2006; Noël et al. 2007, 2009; Weisz et al. 2013; Cignoni et al. 2013, and references therein). Our plan, however, is to obtain CMDs significantly fainter than the oldest MSTO

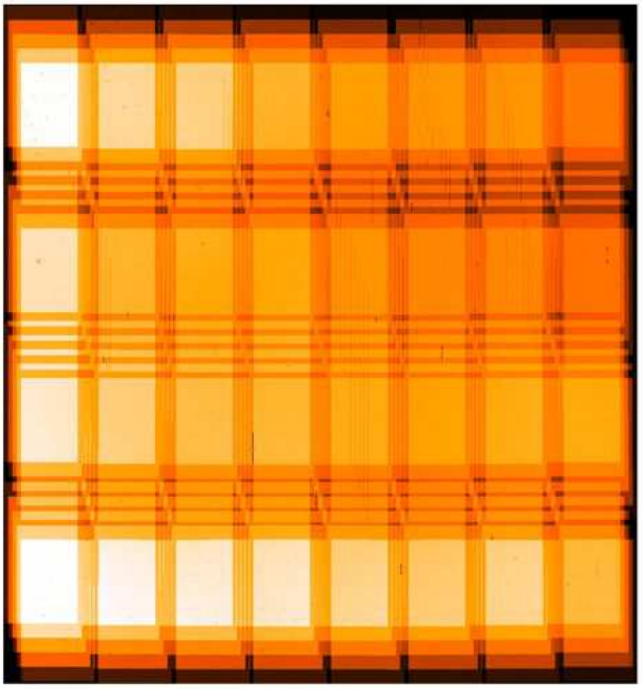

Figure 3. Typical weight map for a VST mosaic ($\sim$ 1 deg^2) obtained with the "5-point diag" pattern using steps of $\pm$25 arcsec in X and $\pm$85 arcsec in Y. The lighter regions are those with higher S/N.

for the entire galaxy, including its halo and the wing in the direction of the LMC. This will allow us to infer for the first time the SFH in a homogeneous way over the whole SMC and over the entire Hubble time.

We intend to use classical variable stars (RR Lyrae, Cepheids, Anomalous Cepheids, δ Scuti etc.) as population tracers, especially in the unexplored region of the Bridge. Indeed, these variable stars provide us insights on the conditions at the epoch of their formation by probing young ages: 50–200 Myr with short and intermediate–period classical Cepheids–CCs; intermediate-ages: $\sim$1–2 Gyr, with the anomalous Cepheids–ACs; and old ages: t $>$ 10 Gyr, with the RR Lyrae stars (for previous similar studies on the SMC body see e.g., Haschke, Grebel, & Duffau 2012; Subramanian & Subramaniam 2012). Eventually, the time-series images are stacked, allowing us to derive deep CMDs and, in turn, to perform a quantitative analysis of the SFH of the investigated tiles (in analogy with the VISTA telescope surveys, hereinafter we call "tile" one single OmegaCAM pointing), completing the information gathered from the analysis of the pulsating stars.

STEP also aims at investigating the first stages of star formation by securing a complete mapping of pre-main sequence (PMS) objects. A survey of young stellar objects in the SMC was conducted with the Spitzer satellite by Sewiło et al. (2013) and HST has already allowed to examine in detail the PMS in a number of SMC regions (Nota et al. 2006; Carlson et al. 2007; Cignoni et al. 2011), but again only with the wide field VST survey we will be able to infer the whole distribution.

STEP will allow us to identify and survey the whole population of SMC star clusters of any type, age and mass above our detection limit. We will make a homogeneous census of the SMC candidate clusters, and thus be able to ascertain whether NGC 121 is indeed the only example of an old system in the SMC, as currently believed, or other as old or possibly older clusters are identifiable (see e.g., Shara et al. 1998; Glatt et al. 2008a).

In summary, STEP will eventually allow us to answer several open questions: 1) Are the trends of SFH with position connected with the interaction history of the SMC? 2) Do field and cluster components share the same SFH? 3) What are the cluster and field age-metallicity relations ? 4) What are the evolution properties of low metallicity stars in the mass range 1-2 $M_{\odot}$? 5) Which is the variable star population of the Bridge? 6) Which is the SFH of the intra-cloud population? 7) How did the stellar component of the Bridge form? By tidal stripping or local formation (Bekki & Chiba 2007; Harris 2007)? 8) What is the impact of metallicity on PMS accretion and on the global properties of star formation (star formation rate and efficiency, and initial mass function)?

There is no other completed or ongoing optical survey on nearby galaxies as deep, wide and panchromatic as STEP. The Magellanic Clouds Photometric Survey (MCPS, see e.g., Zaritsky et al. 2000, 2002; Harris & Zaritsky 2004, and references therein) provided photometry of about 16 deg^2 centred on the SMC. As we shall see in the next sections, compared to MCPS, the STEP survey has the major advantage of observing with a spatial resolution (i.e. CCD pixel-size) 3.5 times higher and with significantly better average seeing conditions. These occurrences mean that STEP can observe stars as faint as $g \sim 22.5 - 23$ mag (i.e. the magnitude of the oldest TO) with uncertainties lower than 10-15% even in the most crowded regions of the SMC. The OGLE III survey (Udalski et al. 2008, see) provides an unpaired amount of information for the variable stars in the SMC body, but, again, it is much shallower than STEP and does not cover the Bridge. The next generation OGLE survey (OGLE IV) covers a wider area around the Magellanic System, including the Bridge, but is still shallower than STEP. The Southern Sky Survey (http://msowww.anu.edu.au/skymapper/survey.php) that is being performed with the Skymapper telescope (Keller et al. 2007), will observe the SMC and the Bridge, but at shallower magnitude limit (g$\sim$22.9 mag with S/N[1]$\sim$5) than STEP and with a worse spatial resolution. Furthermore, their planned 6 epoch sampling is too coarse for an accurate identification and characterisation of the Bridge variables. First results of the Outer Limits Survey, an NOAO survey designed to detect, map, and characterise the extended structure of the MCs, were presented by Saha et al. (2010). However, contrarily to STEP, this survey aims at investigating only the outer regions of the MCs. NOAO observations to further sample the Magellanic stellar periphery have recently began as part of the Survey of the MAgellanic Stellar History (Olsen et al. 2014).

[1] S/N=Signal to Noise

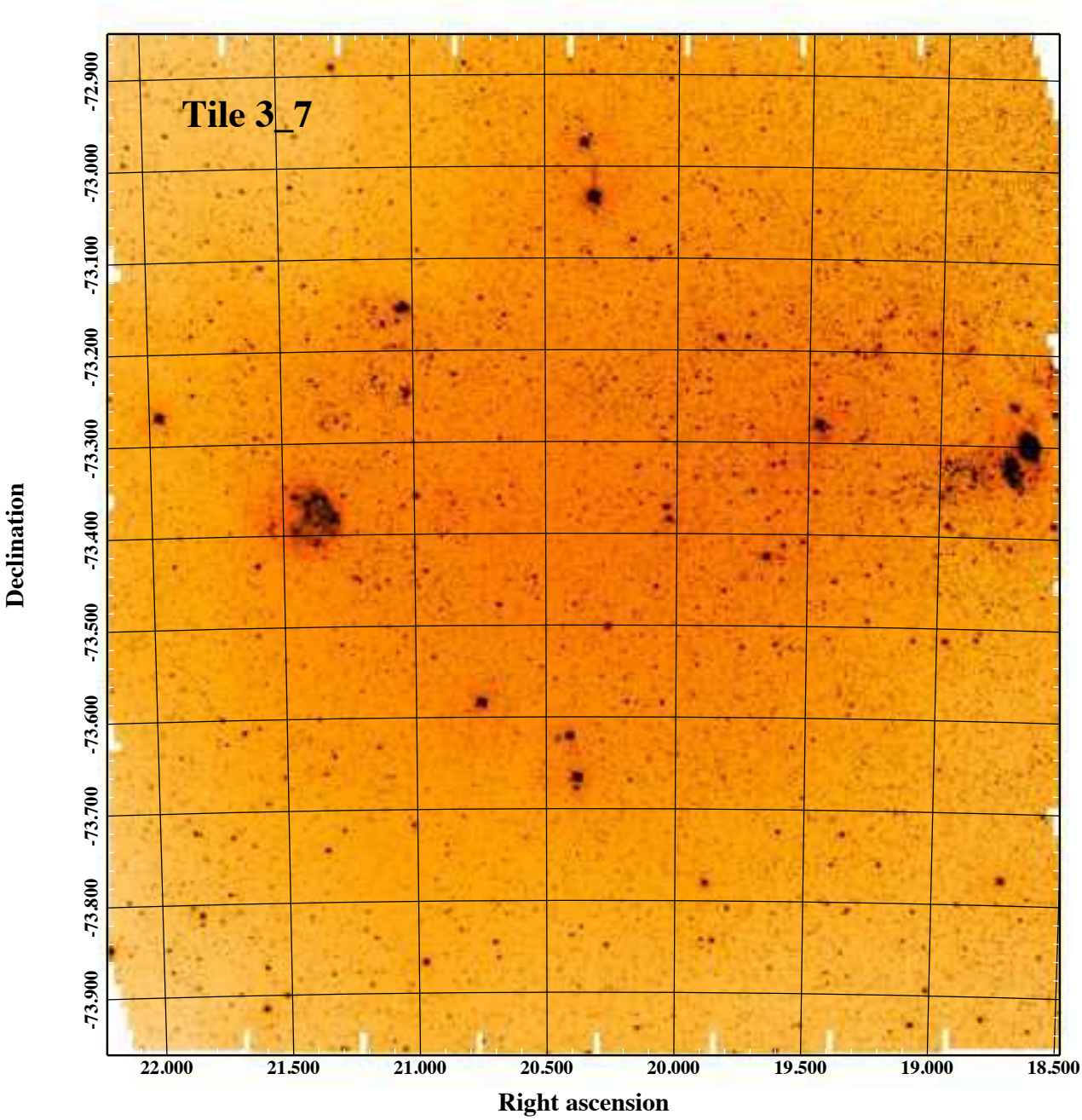

Figure 4. g-band VST plate of tile 3_7. North is up and East is to the left.

2.1 Observing strategy of the STEP Survey

To address the questions listed above, we proposed, and obtained, to use part of the VST GTO time allocated by ESO to Istituto Nazionale di Astrofisica (INAF) in return for the procurement of the telescope and acquire g, r, i, H_α [2] photometry for 72 squared degrees covering the whole SMC body, the Bridge and 2 deg^2 of the Magellanic Stream down to a limiting magnitude (AB system) g ∼24 mag with S/N=10, and r (H_α) ∼ 22.5 mag with S/N=5. The survey is organised with tiles of 1 deg^2 each, partially overlapping with each other to allow a homogeneous calibration.

In addition, we acquired 24-epoch time-series photometry of 8 deg^2 on the Bridge down to $V \simeq 19.5$ mag (i.e. reaching fainter than the mean magnitude of the RR Lyrae stars), with S/N=100. When summed up, these images will allow us to reach g ∼24 mag with S/N=10. Originally, we planned to image with time-series the whole Bridge. However, after the first observations in Period 88 (see below), we found that the huge overheads in pointing and filter changing made the observing efficiency (shutter time/total dura-

[2] See Sect 2.2 for a discussion about the VST filter system

tion of the exposure) so low that we decided to complete only the 8 Bridge fields already started and cover the remaining Bridge fields using the same observing strategy adopted for the SMC body, (i.e., without time-series).

Details on the instrumentation and the observing strategy are reported in the following subsections, while the data reduction is discussed in Sect. 3.

2.2 The VST telescope and OmegaCAM

The VST (built by the INAF-Osservatorio Astronomico di Capodimonte, Naples, Italy) is a 2.6-m wide field optical survey telescope (Capaccioli & Schipani 2011). VST is placed at Cerro Paranal, Chile on the same platform as the VLT 8-m telescopes. VST has a f/5.5 modified Ritchey-Chretien optical layout on an alt-azimuth mounting. It features a two lens wide-field corrector, with the dewar window acting as a third lens (and an optional atmospheric dispersion compensator - ADC) giving a correct FoV of 1 deg^2 (see Schipani et al. 2012). The primary mirror is a concave 2.6 m hyperbolic meniscus axially supported by 84 active supports, placed on four rings and laterally sustained by passive astatic levers. The convex hyperbolic secondary mirror is controlled by a hexapod with 5 degrees of freedom. The telescope is equipped with OmegaCAM, a 1 deg^2 camera build by a consortium of european institutes (Kuijken 2011). The camera is a 32-CCD, 16k x 16k detector mosaic with 0.214 arcsec per pixel scale (for the two-lens corrector, 0.215 for the ADC configuration). The CCDs are thinned, blue-sensitive, 3-edge buttable CCD44-82 devices of high cosmetic quality made by e2v. The field distortion is very low, and the image scale is practically constant over the whole field of view. The gaps between the CCDs are rather narrow, and the overall geometric filling factor of the array is 91.4%.

OmegaCAM can handle 12 filters that can be changed during the night. Currently, the available filters include the Sloan Digital Sky Survey (SDSS) *ugriz* set, Johnson B and V filters, plus several narrow-band filter mosaics such as H_α. It is important to note that the VST filter system is actually based on the USNO $u'g'r'i'$ system (Smith et al. 2002) which is slightly different from SDSS *ugriz* (for details, see Fukugita et al. 1996; Gunn et al. 2001). This is shown in Fig. 1 where the throughput of the filters used in the present survey are displayed and compared with those of the SDSS (properly rescaled to improve the comparison).

However, since we will calibrate our data on the "natural" SDSS system, in this paper we use the *ugriz* notation. The OmegaCAM calibration plan ensures that all data can be photometrically and astrometrically calibrated to 0.05 mag and 0.1 arcsec rms precision, respectively.

2.3 STEP area coverage

The main aim of the survey is to image the body of the SMC and the Bridge. The choice of the survey fields was driven by:

- Complete coverage of the SMC+Bridge area. In particular, we tried to include the classical SMC diameter limit at $B \approx 25$ mag arcsec^{-2} (Bothun & Thompson 1988) as well as major features traced by the distribution of stars, star clusters (e.g., Irwin 1991; Bica et al. 2008) and H I gas (e.g., Staveley-Smith et al. 2003; Hatzidimitriou et al. 2005; Muller et al. 2003), for both the SMC and the Bridge.
- Maximize the overlap with the VMC survey (see Cioni et al. 2011).

In order to accomplish these tasks efficiently we used the Survey Area Definition Tool (Arnaboldi et al. 2008, SADT). A geodesic rectangle with vertexes α=23:53:54; 04:29:30; δ = −75:54:46; −70:02:00 was generated as the basis of the tile creation process. The unnecessary tiles were removed leading to the coverage shown in Fig. 2. This figure shows the 72 tiles (coloured boxes), which define the area surveyed by STEP (apart the two tiles placed into the Magellanic Stream). The tiled area covers almost completely the distribution of stellar clusters and associations (black dots) and maximizes the overlap with the VMC survey (grey boxes).

The coordinates of the centres of each STEP tile are given in Table 2. Each tile is identified by two numbers: the first number gives the row and the second the column of the position of the tile in the mosaic that covers the surveyed area. Row numbers increase from South to North and column numbers increase from West to East.

In the process of defining the mosaic, SADT requires as input the observing parameters that are associated to small (i.e. jittering) and large (i.e. mosaicking) displacements in the tile position. For the STEP survey the maximum jitter was set to 10″, and the tile overlap in α and δ to 120″.

2.4 STEP observations

We can distinguish our observations in "deep" (on the SMC body, on the Wing and on part of the Bridge) and "time-series" (seven fields in the Bridge and one in the SMC periphery). Table 3 describes the main parameters of the VST observations, including the exposure times. For the time-series we decided to take a single exposure per epoch and filter. The images at different epochs of each tile were slightly dithered to cover the gaps between CCDs in the stacked images. As for the deep exposures, we divided the total exposure time, as estimated by the OmegaCAM Exposure Time Calculator (ETC)[3] into 5 or 10 sub-exposures (see Table 3). To avoid saturation for the bright SMC/Bridge stars we also acquired 5 short (25 s each) exposures per tile. We chose the same dithering pattern for both time-series and deep exposures. In particular, we adopted the "5-point diag" pattern[4] which offsets the telescope by the same amount between successive exposures. The size of the steps in X and Y directions is as large as the largest gap in the mosaic, i.e. about ±25 arcsec in X and ±85 arcsec in Y. A typical weight map for the stacked tile is shown in Fig. 3, where the brighter regions are those with larger S/N. Although the weight map is provided as output by the VST–Tube package, we did not use it in the derivation of the photometry (see next sections).

For the deep images we required clear sky, but we allowed for thin–cirrus for the time–series photometry, to in-

[3] http://www.eso.org/observing/etc/bin/gen/form?INS.NAME=OMEGACAM+INS.MODE=imaging

[4] See the omegaCam template manual, document available at http://www.eso.org/sci/facilities/paranal/instruments/omegacam/doc/VST-MAN-OCM-23100-3111-2_7_1.pdf

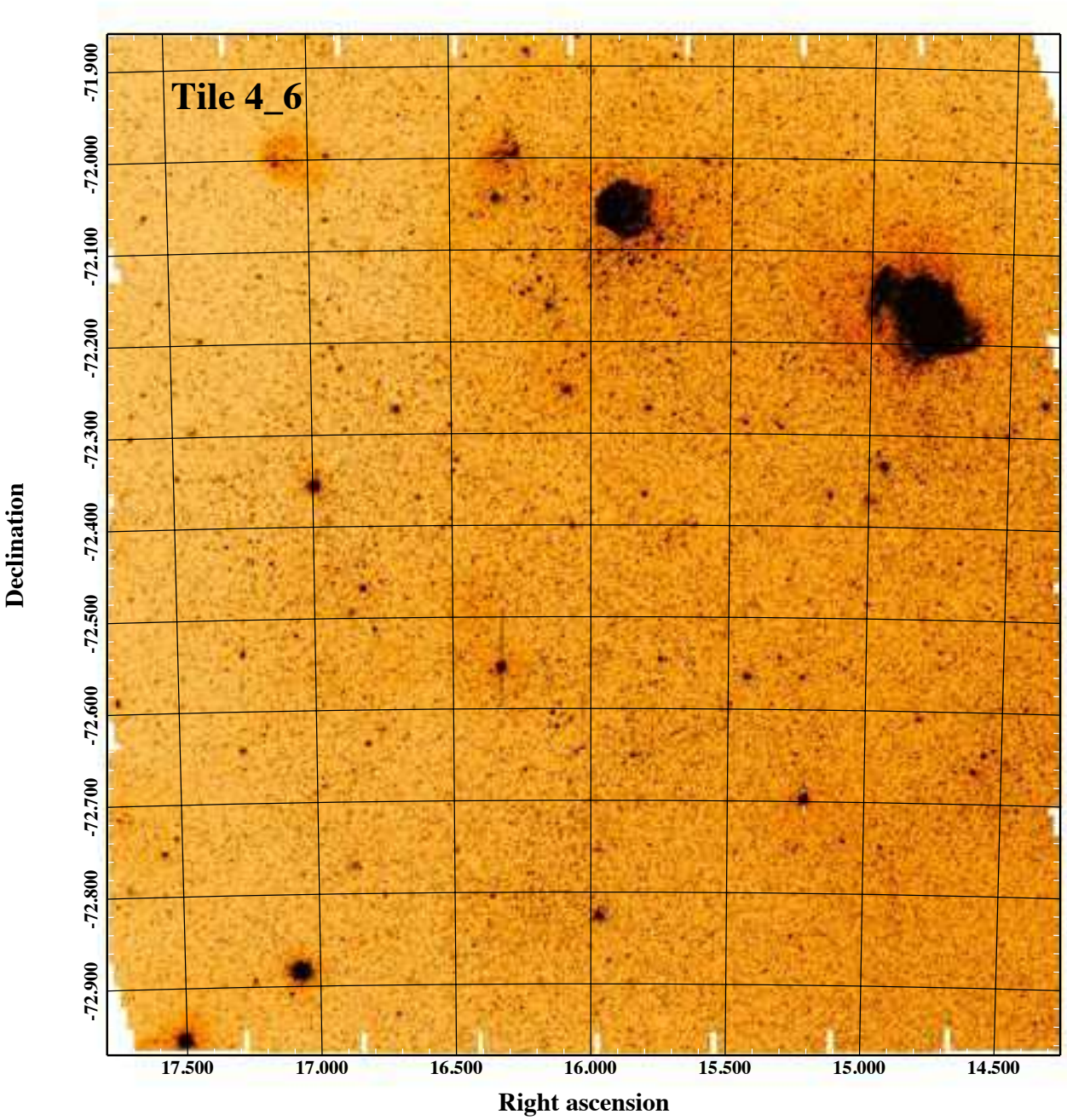

Figure 5. *g*-band VST plate of tile 4_6. North is up, East is to the left.

crease the probability of program execution. Moreover, images obtained in each of the two filters were left free to be acquired in different nights. Hence, to perform the photometric calibration of the data we need secondary standard stars. For time-series tiles this was secured by requiring that at least two of the epochs were taken under photometric condition. To calibrate the deep tiles, instead, we planned for a couple of short exposure g, i images (see Table 3) to be acquired during a photometric night. These images were sufficiently deep to provide a huge amount of stars to be used as secondary standards.

Finally, we exploited the overlap between adjacent tiles to correct for residuals in the photometric zero points. The overall zero point of the photometry was checked using calibrations obtained during different observing runs.

Most of the observations of the STEP Survey are obtained in service mode by ESO staff. This guarantees efficiency of operations and a high level of data homogeneity. Only a few hours of observation were conducted in visitor mode (GTO compensation time).

The constraints on the observing conditions varied as a function of the crowding of the target regions. In general, for the SMC body and the Wing we required a better seeing

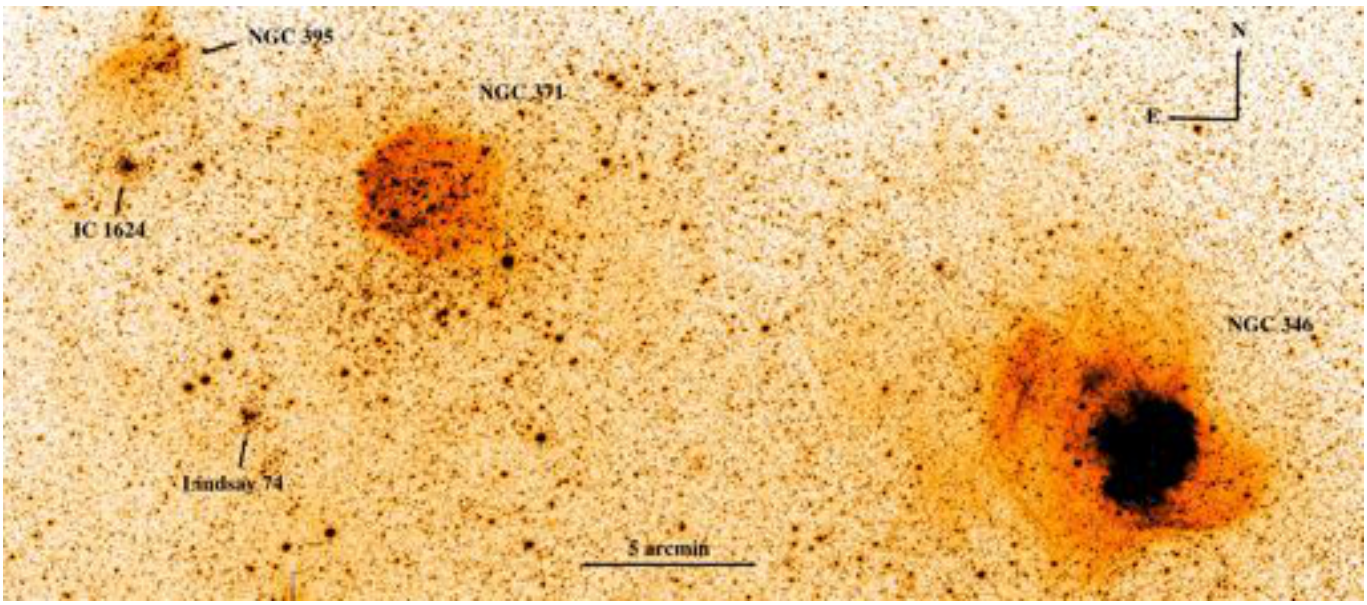

Figure 6. Enlargement of Fig. 5 showing the northern part of tile 4_6, including the well known star forming region NGC 346 and several other interesting clusters and associations which are labelled in the figure.

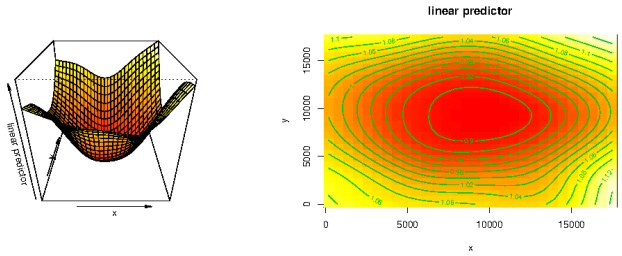

Figure 7. Left: IC 3D view; Right: Contour plot of the IC image

Table 3. Observing Strategy

Period	$T_{exp}(g)$	$T_{exp}(i)$
88-90	5×25 s; 5×520 s	5×25 s; 5×520 s
91-92	5×25 s; 10×300 s	5×25 s; 10×300 s
Photometric calibration		
88-92	1×45 s	1×45 s
Time-Series		
88-91	1×25 s; 1×120 s	1×25 s; 1×180 s

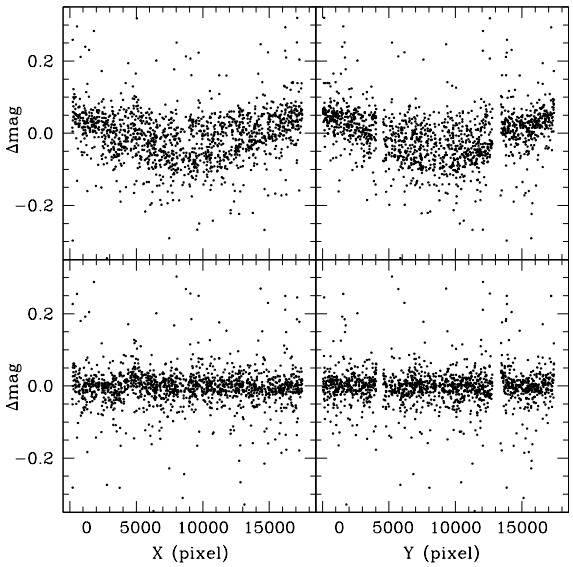

Figure 8. Residuals (VST-SDSS) vs x and y position before (top panels) and after (bottom panels) the IC correction

than for the less crowded tiles in the Bridge. A summary of the observing constraints is provided in Table 4.

Since the SMC and the Bridge never rise above 50° from the horizon, the seeing measured on the images is expected to be significantly larger than that measured at the Zenith. Hence to keep a reasonable probability of realisation of the observations, we decided to accept a seeing limit of 1.0″–1.1″ (corresponding to ∼0.7″ at the Zenith) even for the crowded body of the SMC. These values of seeing allow us to reach our scientific goal in terms of magnitude limit.

A more relaxed constraint of 1.4″ seeing was used for

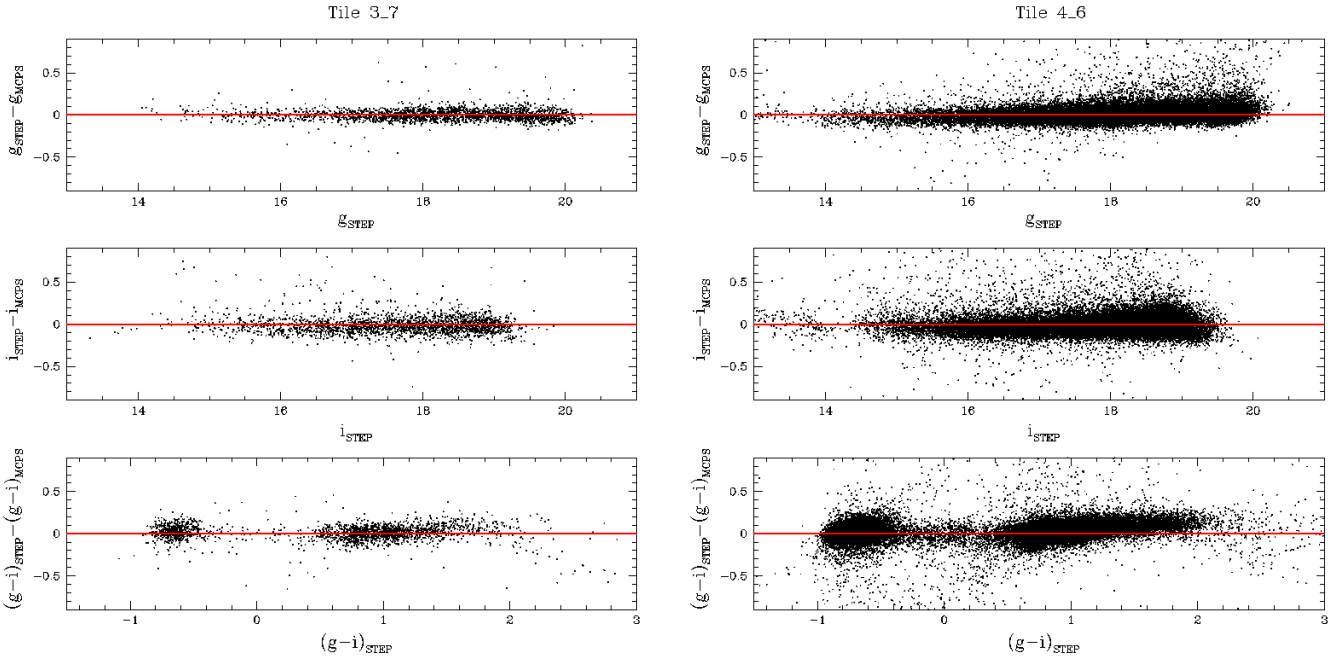

Figure 9. Comparison between STEP and MCPS photometries (transformed to the SDSS system according to Jordi, Grebel, & Ammon 2006, colour conversions).

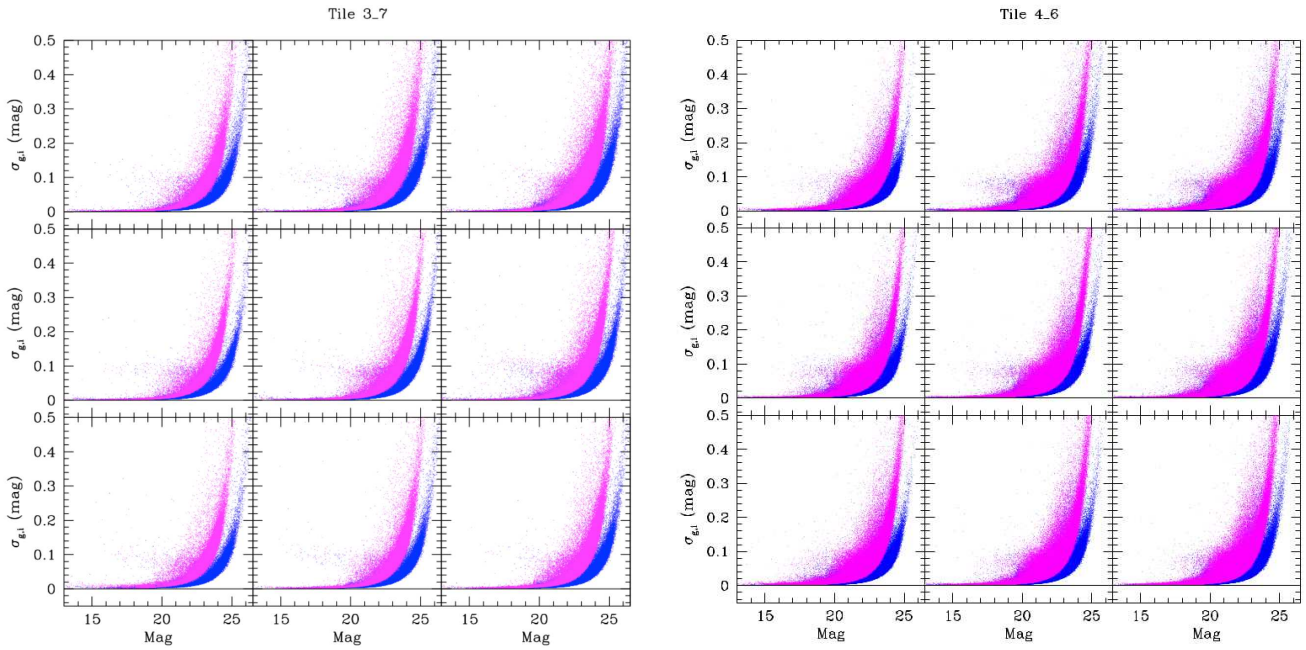

Figure 10. Photometric errors in g (blue) and i (magenta) for tiles 3_7 and 4_6. To verify the presence of possible differences within each image, the tiles were divided into nine sub-frames $20' \times 21'$ each. North is up and east on the left

the uncrowded regions of the Bridge to be imaged in time-series mode. For the Bridge tiles to be observed with one epoch deep images, this constraint was reduced to $1.1''$ to account for the shorter total exposure time with respect to those obtained by summing up all the time-series images.

The efficiency (hours of actual observations/hours allocated) of the STEP observations is shown in Table 5. A quick comparison of columns 2 and 3 reveals that, at face value, the observing efficiency was of the order of 54%. However it can be noticed that the actual efficiency was significantly lower. Table 5 also reports the average grade[5] from Period 88 to 91.

[5] For the meaning of the various grades see http://casu.ast.cam.ac.uk/surveys-projects/vista/data-processing/eso-grades

Table 4. Observing constraints. Seeing is to be intended as the full width at half maximum measured on the image. TS stands for time-series.

Field	Seeing	Moon	Airmass	Weather
SMC	1.0″–1.1″	0.5	1.8	Clear
Bridge	1.1″	0.5	1.8	Clear
Bridge (TS)	1.4″	0.8	1.8	Thin cirrus
Phot. Cal.	1.5″	0.8	1.8	Photometric

Table 5. Distribution of the observations in the ESO Periods (column 1). Columns (2) and (3) show the hours allocated and those actually devoted to the observations, respectively. Column (4) list the efficiency (in percentage) of the observations, i.e. the ratio col. (3)/col. (2). Column (5) shows the percentage of OBs graded by ESO as A,B,D. See text for a detailed explanation.

Period	Allocated (h)	Observed (h)	Obs./Allocated (%)	Grade A,B,D (%)
(1)	(2)	(3)	(4)	(5)
88	40	9.8	24.5	16,30,54
89	43	37.2	86.5	19,37,44
90	34	24.8	73	29,65,6
91	49	19.7	40	20,44,36
92	16	7.2	45	50,32,18
93	18			
	Total	Total	Average	Average
88-92	182	98.7	54	27,42,31

It can be seen that grades "A" and "B" were obtained only in 27% and 42% of the cases, respectively. The remaining 31% of the images was graded as "D", i.e. with characteristics that are by more than 20% outside the limits we had set, in terms of seeing and/or ellipticity. This last occurrence is particularly harmful because it prevents us from obtaining a good astrometric solution for the images composing one mosaic, making the tiles sometimes completely useless, and to be re-observed in the following semester. Hence, even if the observing efficiency of the STEP observations was formally of 54%, the survey efficiency, i.e. the percentage of useful data, was well below 50%.

2.5 STEP progress

As shown in Table 5, STEP observations started on P88. Time-series photometry was collected till P90. The number of epochs for each tile is listed in Tab. 6. Given the extremely low efficiency (shutter time/total duration of OB) of this kind of observations (as low as 25%) we decided to acquire only deep tiles starting from P91.

As for the deep tiles, at the moment of writing, there are 16 tiles completed (see Table 2 and Fig. 2), whereas several additional tiles were so far only partially observed

Table 6. Number of epochs for each tile observed by means of time-series photometry.

Tiles	n_{epochs} (g)	n_{Epochs} (i)
5_9	26	23
2_10	23	22
3_12	24	23
3_13	24	23
3_14	23	22
3_15	21	20
3_17	22	21
3_19	21	20

(see Table 2). The observations in r, H_α will start as soon as the g, i survey is completed.

2.5.1 The first two completed tiles.

We have chosen to give highest priority to observations of two tiles which include fields already observed by our group with the HST Advanced Camera for Surveys (ACS): one in the most active region of the SMC main body and the other in the most external regions of the Wing. The former is tile 4_6, around the very young cluster NGC 346, and the latter is tile 3_7 in the Wing. They cover the NGC 346 and the SFH9 ACS fields observed respectively by the HST programs 10248 (PI Nota, see Nota et al. 2006) and 10396 (PI Gallagher, see Sabbi et al. 2009). This allows an immediate comparison of the VST photometry with the exquisite one from ACS, as well as an independent check on the calibration. The plates shown in Figures 4 and 5 report the OmegaCAM@VST mosaic images relative to tiles 3_7 and 4_6, respectively. Figure 6 exhibits an enlargement of the northern part of plate 5, including the well known star forming region NGC 346 and several other interesting clusters and associations.

Since STEP covers the whole SMC, it will eventually include not only all our HST fields, but also those studied and published in the astronomical literature, both from space and from the ground.

3 DATA REDUCTION

In this section we describe the procedure adopted for the treatment of the raw data and the production of the final catalogue ready for the scientific exploitation. In the following we refer mainly to the deep exposures. Details on the treatment of time-series data will be provided in a dedicated paper.

3.1 Pre-reduction, astrometry and photometric calibration

The images of tiles 3_7 and 4_6 were collected during different runs (see Table 7 for details). The data reduction has made use of the VST–Tube imaging pipeline (Grado et al.

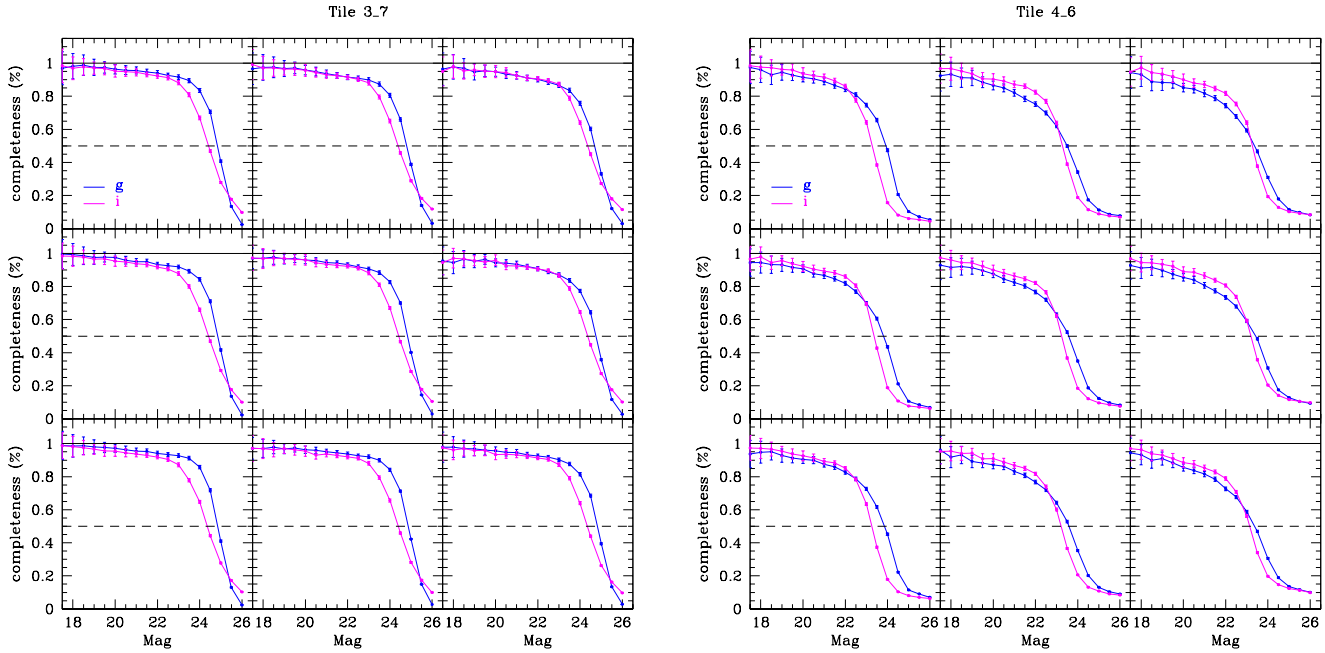

Figure 11. Completeness for the tiles 3_7 and 4_6 (blue and magenta solid lines refer to g and i bands, respectively). To verify the presence of possible differences in completeness within each image, the tiles were divided into nine sub-frames $20' \times 21'$ each. North is up and east to the left. The 100% and 50% levels of completeness are shown with black solid and dashed lines, respectively.

2012), installed and running on the computers of the INAF–VST Center (VSTCeN[6] hosted by the INAF-Osservatorio Astronomico di Capodimonte, Naples). This pipeline was specifically developed for the VST telescope but is available also for other existing or future single or multi-CCD cameras. Removal of instrumental signatures that include overscan, bias and flat-field correction, CCD gain equalisation and illumination correction have been applied. Relative and absolute astrometric and photometric calibration were applied before stacking for the final co-added image. In detail, the overscan correction uses the median value of the overscan region portion and the master-bias comes from a sigma-clipped average of bias frames. The gain variation over the field of view is obtained using a suitable combination of twilight flat-fields and science images (with large enough dithering) as given by the formula:

$$MFlat = Imsurfit\left(\frac{SFlat}{TFlat} < TFlat >\right) TFlat \times \mathrm{IC} \quad (1)$$

where $MFlat$, $SFlat$, $TFlat$ stands for Master-Flat, Sky-Flat and twilight-flat, respectively. $Imsurfit$ is a Chebyshev polynomial image fit, whereas IC (Illumination Correction) is an analytic function reproducing the image concentration effect. TFlat images are first corrected by overscan and then corrected by the master-bias. The average Tflat is produced using a sigma clipped prescription. < TFlat > is a median computed on an inner region of the TFlat. The Sky-Flat is produced with the same procedure as the TFlat but using science images. The Sky-Flat is used to correct the large scale variations due to non-uniform illumination and the high S/N TFlat is used to correct the high-frequency pixel to pixel sensitivity variations.

To have the same zero-point for all the mosaic chips, a gain equalisation procedure has been used. The procedure finds the relative gain correction which gives the same background level in adjacent CCDs. For the OmegaCAM@VST images it was necessary to apply a further correction caused by scattered light. This is frequent for wide field imagers where telescope and instrument baffling can be an issue. This results in a centrally localised additive component to the background, and the flat field does not accurately estimate of the spatial response of the detector. Indeed, if not corrected, after flat-fielding the image background would appear perfectly flat but the photometric response would be position dependent (Andersen, Freyhammer & Storm 1995). This error can be mitigated through the determination and application of the IC map. The IC map was derived using SDSS DR8 stars in properly selected fields. The magnitude residuals (VST-SDSS) as function of the position were fitted using a generalised adaptive method (GAM) in order to obtain an IC map used to correct the science images during the pre–reduction stage. The GAM allows to obtain a well behaved surface also in case the field of view is not uniformly sampled by standard stars. As an example we show in Figures 7 and 8 the IC map and the position dependency of the zero-point before and after the IC application.

The absolute photometric calibration was computed on the nights reported in Table 8 comparing the observed magnitude of standard stars with SDSS photometry.

In Tab. 8 we report the zero-points and colour terms obtained using the Photcal tool[7]. Since the photometric

[6] http://vstportal.oacn.inaf.it/

[7] http://www.na.astro.it/ radovich/

standard star fields were observed with a span in airmass too small for a suitable fit, an average value for the extinction coefficient was adopted. Relative photometric correction among the exposures is obtained by minimising the quadratic sum of the differences in magnitude between overlapping detections. The tool used for such task is SCAMP (Bertin 2006). Absolute and relative astrometric calibration is performed using SCAMP as well. Resampling for the application of the astrometric solution and final image coaddition has been obtained using SWARP (Bertin 2002).

We note that the lack of a significant number of standard stars with $(g-i) < 0.0$ mag makes it difficult to constrain the photometric calibration in the colour range -0.7< $(g-i)$ <0.0 mag. For this reason, the photometric calibration for stars with the bluest colours, corresponding to the young stellar populations in the SMC, could be less accurate than for stars in the colour range 0.0< $(g-i)$ <2.5 mag. We are working to solve this problem by observing a significant number of blue stars in the Stripe 82 standard field (Ivezić et al. 2007). These observations will allow us to accurately constrain the colour terms in the calibration equations. In the meantime, we can check quantitatively the goodness of our photometry by comparing our data with those from the MCPS survey. To this aim, we have first to transform the MCPS BVI photometry into SDSS g, i. This can be achieved by adopting the Jordi, Grebel, & Ammon (2006) results[8] for population I objects, as the metallicity of the SMC is closer to population I than population II stars. We note that these transformations are nominally valid for $(V-I) < 1.8$ mag, i.e. $(g-i) < 2.1$ mag, however, it is not clear which is the validity boundary towards blue colours. Secondly, we have matched the STEP and MCPS catalogues accepting stars within $1''$ and with S/N$\geqslant$20 in each band (for both surveys). The result of this comparison for tiles 3_7 and 4_6 is shown in Fig. 9. These figures show that there is a fairly good agreement between the two photometries. Even if a significant scatter ($\sim$0.08 mag) is present the formal average differences (in the sense STEP-MCPS) are: $\Delta g(3\_7) \sim -0.004$ mag; $\Delta i(3\_7) \sim -0.018$ mag; $\Delta(g-i)(3\_7) \sim +0.014$ mag; $\Delta g(4\_6) \sim +0.014$ mag; $\Delta i(4\_6) \sim -0.014$ mag; $\Delta(g-i)(4\_6) \sim +0.027$ mag. The maximum deviation is less than 3% in color in tile 4_6, confirming the absence of significant photometric errors on the calibration.

3.2 Photometry

Our fields present different levels of crowding. The SMC body, in particular, is heavily congested with stars. This requires the use of Point Spread Function (PSF) photometry. We employed the package DAOPHOT IV/ALLSTAR (Stetson 1987, 1992) and the PSF function was left to vary across the FoV. Usually a first or second order variation of the PSF with radial position was sufficient to recover star shapes even at the edges of the tiles.

[8] **For ease of use, we adopted Jordi, Grebel, & Ammon (2006)'s transformation equations in the form available at http://www.sdss3.org/dr8/algorithms/sdssUBVRITransform.php.**

Table 7. Observing Log for tiles 3_7 and 4_6.

tile	filter	Date (UT)	Exp. Time (sec)	seeing ($''$)
3_7	g	2012/10/13	125s; 2600s	0.95
3_7	i	2012/10/13	125s; 2600s	0.85
3_7	g, i Cal.	2012/08/14	45s	2.1,1.8
4_6	g	2012/09/20	125s; 2600s	1.05
4_6	i	2012/08/9	125s; 2600s	0.85
4_6	g, i Cal.	2012/08/14	45s	1.7,1.2

Table 8. Absolute photometric calibration for tiles 3_7 and 4_6 (rows 1,2 and 3,4, respectively). The colour term is with respect to $(g-i)$. These coefficients are accurate for $(g-i) > 0$ mag. The formal uncertainty on zero-points (ZP) and colour terms are also shown. The date format is dd mm yyyy.

tile	band	ZP mag	Col. term mag	extinction mag/airmass	date
3_7	g	24.767±0.016	0.016±0.013	0.18	13 09 2012
3_7	i	24.094±0.014	-0.003±0.011	0.043	13 09 2012
4_6	g	24.832±0.015	0.015±0.012	0.18	20 09 2012
4_6	i	24.107±0.007	-0.003±0.006	0.043	09 08 2012

At the end of the pre-reduction procedure we were left with three images for each filter and deep tile. Two are mosaics resulting from the stack of the short and long exposures, respectively (see Tab. 3), the third image is the single shot acquired to produce secondary standard stars. Each image was measured separately. For each filter the output short and long exposure files were matched to adjust the residual photometric zero point difference (usually of the order of 0.01-0.015 mag) by averaging the photometry of the stars in common. This match was performed in α and δ, which were calculated from the ALLSTAR x,y physical coordinates using the World Coordinate System (WCS) of the images and the package *xy2sky*[9]. For the match we used the *STILTS*[10] package setting a tolerance in both α and δ of $0.25''$, i.e. slightly more than 1 pixel. The resulting g, i catalogues were matched in the same way, allowing us to obtain a unique catalogue including all the photometry for each tile.

Similarly, the pair of g, i single exposures acquired with the purpose of providing secondary standards, were matched. For all the stars in common we then applied the colour terms listed in Tab. 8 (we recall that the zero point is already photometrically calibrated by the VST–Tube pipeline), obtaining the desired secondary standard stars.

Finally, the last step of the whole procedure was the refinement of the photometric calibration. This is achieved by matching the catalogue of the secondary standard stars with

[9] http://tdc-www.harvard.edu/wcstools/xy2sky/
[10] http://www.star.bris.ac.uk/ mbt/stilts/

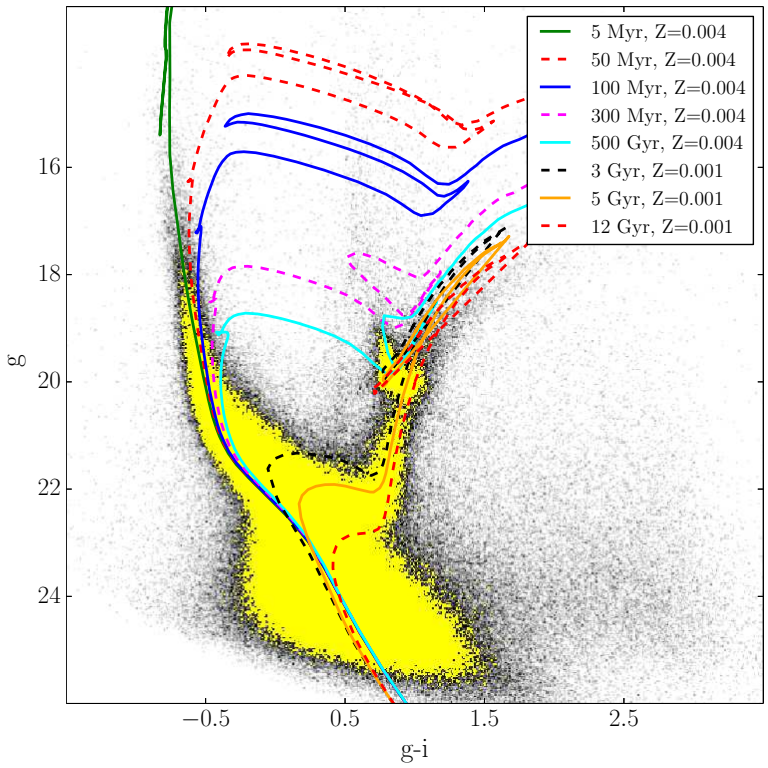

Figure 12. CMD of tile 3_7 with overlaid Marigo et al. (2008) stellar isochrones for metal abundance Z=0.004, ages 5 Myr (green continuos line), 50 Myr (red dashed line), 100 Myr (blue continuous line), 300 Myr (pink dashed line) and 500 Myr (cyan continuous line); Z=0.001, ages 3 Gyr (black dashed line), 5 Gyr (orange continuous line), and 12 Gyr (dashed red line). Assumed distance modulus and reddening E(B-V) are 18.9 mag and 0.08 mag, respectively.

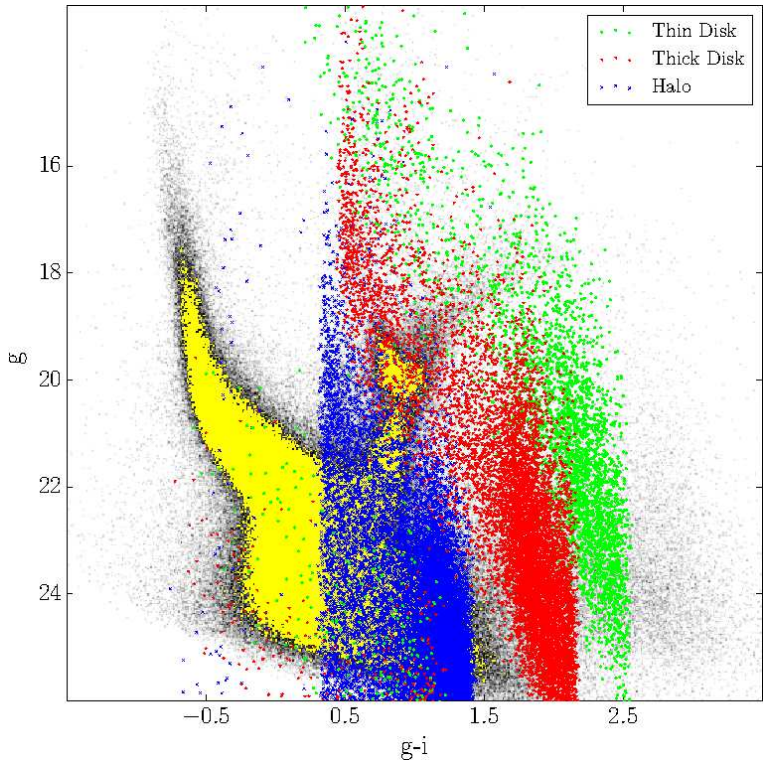

Figure 13. CMD of tile 3_7 with overlaid a simulation of MW contamination expected in the FoV. Halo stars are in blue, Thick disk stars in red and thin disk stars in green.

that including all the photometry of the tile and correcting for the possible difference in zero points. Since most of the data have been acquired in "clear" conditions, corrections were found to be small, of the order of a few percent.

To show the quality of the photometry, we report in Fig. 10 the errors provided by ALLSTAR in g and i as a function of the magnitude for the nine sub-frames in which we virtually divided each tile with the aim of identifying possible differences in the behaviour of the photometric errors.

3.3 Completeness

A detailed estimate of the completeness of our photometry is a fundamental step for an accurate reconstruction of the SFH (see e.g., Tosi et al. 2001, and references therein). We followed the usual procedure of adding artificial stars to the images and calculating the percentage of the recovered stars. More in detail, the steps of our procedure were the following:

- The colour, the magnitude and the relative frequency of the stars to be inserted in the images were calculated on the basis of a synthetic CMD roughly representing a population characteristic of the SMC and Bridge. The range of magnitude taken into account was $14<g<26.5$ mag and the total number of artificial stars was about 2 millions for each tile, distributed along many different completeness experiments (see next point).
- To avoid self-crowding, we sub-divided the images in virtual boxes 70x70 pixels in size each. One artificial star is placed inside each box at random position, so that we can place several thousands of artificial stars avoiding the problem of self-crowding.
- A star is considered as recovered if it is measured both in g and i and if its position and magnitude are returned within $0.25''$ and 0.75 mag of its input values, respectively.

The result of this procedure is shown in Fig. 11 for the two tiles presented in this paper. To verify the presence of possible differences in completeness within each image, the tiles were divided into nine sub-frames $20'\times21'$ each. The completeness in g and i are represented with different colours. The figure shows that the magnitude level corresponding to 50% completeness is brighter ($g\sim23.5$ mag) for tile 4_6, that is much more crowded than tile 3_7 ($g\sim24-24.5$ mag). It is instructive to compare these values with those obtained with HST by Sabbi et al. (2009) for the fields SFH9 and SFH4, included in the tiles 3_7 and 4_6, respectively. Indeed, an inspection of their Figure 3 reveals that for HST data 50% completeness was reached at $V\approx26.2$ mag, $I\approx26$ mag and $V\approx24$ mag, $I\approx25.2$ mag for fields SFH9 and SFH4, respectively. Even if the g and V magnitudes cannot be directly compared, we can roughly conclude that VST data become severely incomplete at about 1-1.5 mag brighter than with the HST photometry.

Artificial stars also provide a realistic estimate of the photometric error, hence the best age resolution achievable within STEP. In the range $22.5<g<23$ mag (approximately the magnitude of the oldest TOs in the SMC), tile 4_6 is characterised by a photometric accuracy in g magnitude of about 0.2 mag. This translates into a maximum precision of $\sim17\%$ in the derived ages (see Vandenberg & Bell 1985), which is equivalent to an age error of 1.7 Gyr at 10 Gyr. For tile 3_7, however, crowding conditions are less severe and the age error at 10 Gyr drops at about 1 Gyr. Although these performances are not comparable with those reached with HST, they are superior to the performances of the MCPS, where the maximum age resolution at 10 Gyr is worse than 3 Gyr.

4 THE STELLAR POPULATIONS IN THE CENTRAL AND WING REGIONS

As planned by our observing strategy, the first STEP fields for which data acquisition was completed were tile 4_6, around the very young cluster NGC 346, and tile 3_7 in the wing. As described in Section 2.3, field 3_7 includes our HST/ACS field SFH9, while field 4_6 covers our HST/ACS pointing on NGC 346 and also overlaps with the ESO Public Survey VMC tile SMC 5_4.

4.1 Tile 3_7

4.1.1 CMD

The CMD of all the stars measured in tile 3_7 is displayed in Fig. 12. There are a number of stellar evolution phases easily identifiable in the CMD, including a well defined and extended MS, a prominent RC (visible at $0.75<g-i<1$ mag and $19.7<g<20.2$ mag) and a blue loop (BL; mostly visible at $0.7<g-i<0.9$ mag and $19<g<19.5$ mag).

There are also contaminants. Figure 13 shows the data CMD with overlaid a simulation[11] of the MW foreground expected in tile 3_7, according to the Galactic model for star counts described in Castellani et al. (2002) and Cignoni et al. (2007). Different colours represent the three major galactic components, namely Halo (blue), Thick Disk (red) and Thin Disk (green). According to this comparison we suggest that in the CMD of Fig. 12, the group of stars in the colour range $1.75<g-i<3$ mag and $g>20$ mag and the vertical sequence at $g-i\approx0.6$ mag and $g<18$ mag are likely foreground MW stars along the line of sight. However, it is also noteworthy that simulations do not show MW stars redder than $g-i\approx2.5$ mag, while observations reach $g-i\approx3$ mag and beyond. Although there are known theoretical problems to reproduce observed stellar colours at such low temperatures, we suggest that part of the mismatch is due to background galaxies. Indeed, using near-infrared VISTA observations for LMC fields, Rubele et al. (2012) find unequivocally that background galaxies are important contaminants, dominating star counts for $Y-K_s>2$ mag and $K_s>17$ mag, while MW foreground stars are concentrated at $Y-K_s\approx$ 1-1.5 mag.

In Fig. 12 isochrones of different ages and metallicities from Marigo et al. (2008) are overlaid to the CMD. The metallicity of the youngest isochrones is assumed to be Z=0.004, which is consistent with spectroscopic derivations from HII regions in the SMC (see e.g., Russell & Bessell 1989; Kurt & Dufour 1998) and from stellar abundances of very young stars (see e.g., Gonzalez & Wallerstein 1998; Hunter et al. 2007, 2009; Bouret et al. 2013), while the metallicity of the older isochrones (Z=0.001) is chosen

[11] Photometric errors and incompleteness are not included.

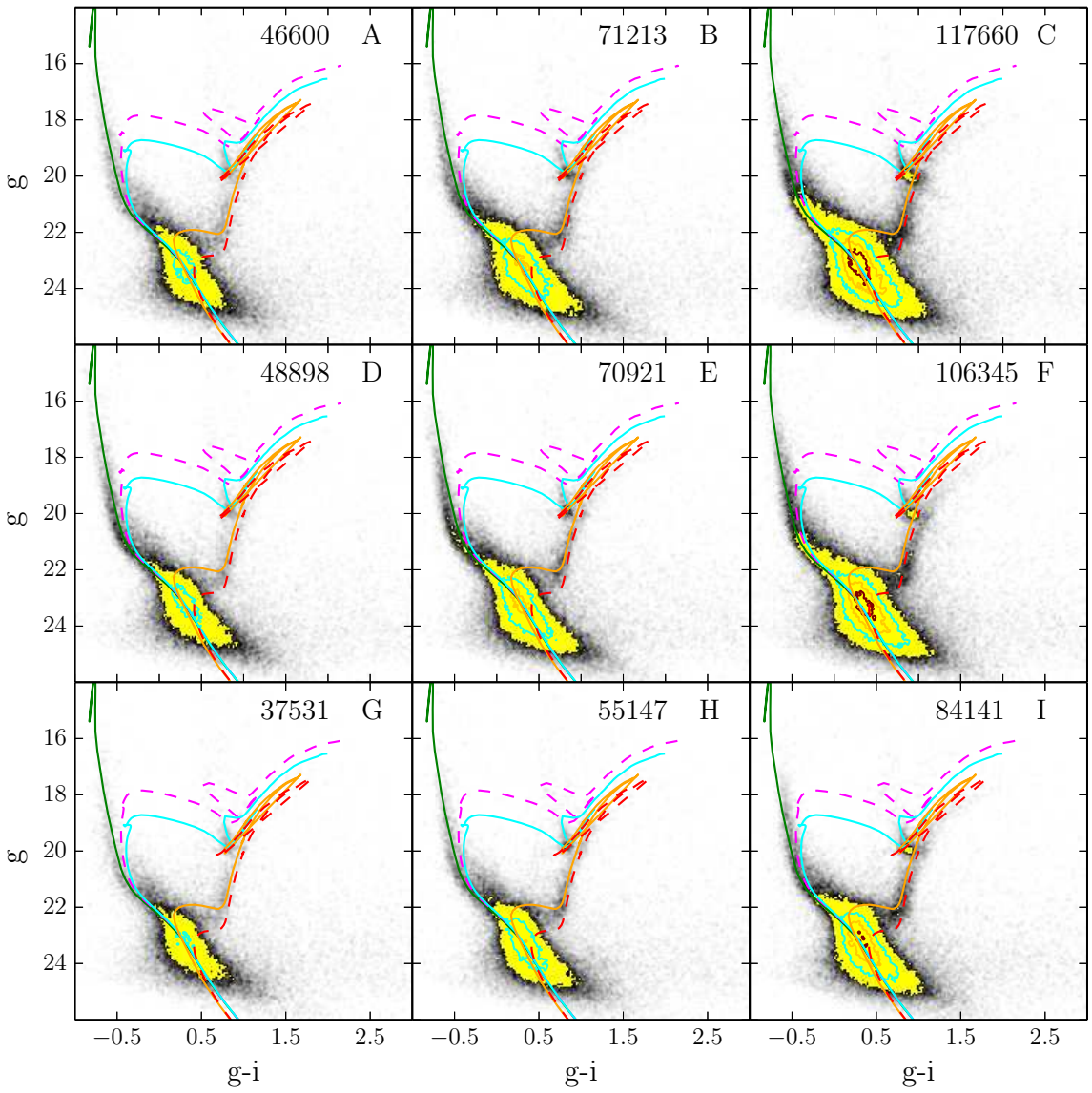

Figure 14. CMDs for nine $20' \times 21'$ arcmin subregions of tile 3_7. The isochrone ages and metallicities are the same as in Figure 12. Assumed distance modulus and reddening E(B-V) are 18.9 mag and 0.08 mag, respectively.

to best fit the RGB (see e.g., Butler, Demarque, & Smith 1982; Haschke et al. 2012). The assumed distance modulus is $(m-M)_0 = 18.90$ mag (see e.g., Harries et al. 2003), while the reddening value is E(B-V)=0.08 mag.

The presence of bright MS stars, BL and RC stars provides circumstantial evidence that tile 3_7 has been actively forming stars for the last few Gyrs. Moreover, the conspicuous number of upper-MS (UMS) stars between the 5 Myr and 100 Myr isochrones suggests that the region went through a recent intense star formation phase producing such massive stars. Looking back in time, the next relevant feature is a rather short BL, roughly consistent with a 400-500 Myr old population, while the paucity of BL stars brighter than $g = 19$ mag suggests a reduced star formation 100-300 Myr ago. The RC is roughly round and well populated, which implies a continuous activity at intermediate epochs. On the other hand, there is no evidence for an extended or even red HB, suggesting a very low star formation rate earlier than 10 Gyr ago. Overall, these results compare well with previous investigations of the region. Using deep HST/ACS data, Cignoni et al. (2013) studied the detailed star formation of a field (SFH9) included in tile 3_7. Their results show a broadly constant intermediate age activity (1-7 Gyr ago), with a recent burst of star formation overimposed, and very modest activity in the first few Gyr.

In order to better visualize the variation of extinctions and crowding conditions, we divided tile 3_7 into nine sub-regions $20' \times 21'$ arcmin large, and compared their CMDs (see Fig. 14) to the same set of isochrones. The old isochrones bracket well all the observational RGBs, except in subregions C and F where the foreground reddening is probably higher.

On the other hand, the blue edge of the MS appears often bluer than our youngest models (see e.g. subregion E). Adopting a slightly lower metallicity or reddening could mitigate this effect, but would cause other inconsistencies.

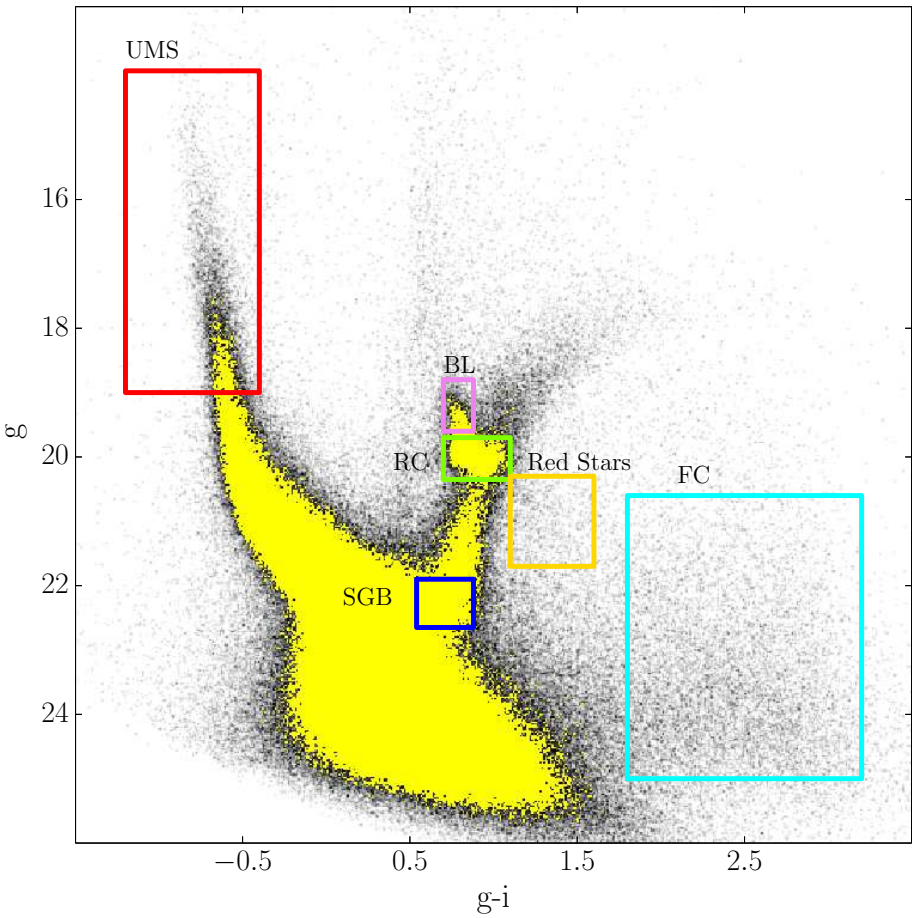

Figure 15. Tile 3_7. CMD regions used to isolate UMS, BL, RC, SGB, reddened RC stars and FC sources.

In fact, the adopted metallicity (Z=0.004) provides excellent fits to the MS derived from HST data (see e.g., Cignoni et al. 2012, 2013). Moreover, younger populations are generally more reddened than older ones (see e.g., Zaritsky et al. 2002), while the data would require the opposite. We do not elaborate further on this issue because of possible problems in the calibration of blue stars. As discussed in Sect. 3.1 this aspect will be improved in future papers. Here our main aim is only to show the full potential of the STEP survey.

4.1.2 Spatial distribution

The spatial distribution of stars in different evolutionary stages yields important information on the star formation processes over the region. We have counted stars in different age regions of the CMD (see Fig. 15), sampling the UMS (red box), RC (green box), BL (pink box) and sub-giant branch (SGB, blue box) stars. Field contamination (FC; interlopers from the MW and background galaxies) and highly reddened RC stars are sampled with the cyan and yellow boxes, respectively. Fig. 16 shows the spatial distributions of these different groups of stars.

From the spatial point of view, we note that populations grow more compact as one moves toward younger ages. In particular:

- UMS stars (top left panel in Fig. 16) appear clumpy and irregularly distributed. Two major concentrations are visible at (α = 21.1, δ = −73.2) and (α = 18.9, δ = −73.3). In terms of age, this implies that most of the ongoing and recent (i.e. in the last 100 Myr) star formation is concentrated in these locations, while the activity is stagnant in the rest of the field;
- BL stars (top right panel in Fig. 16) appear more evenly spatially distributed than UMS stars, but still a bit clumpy. However, given the paucity of these objects compared to UMS stars (ten times more numerous), it is difficult to assess the significance of the various structures, except the mild gradient of increasing concentration toward the upper-right corner of the FoV, which is clearly overdense with respect to the opposite corner. Physically, this implies that either star formation younger than 500 Myr and older than few Myr (the minimum age of BL stars) is occurring on extended scales, not just in few clumps like the UMS, or that stars have been able to disperse during this length of time.
- Overall, RC stars (middle-left panel) follow the spatial distribution of BL stars, but are more evenly distributed along the δ axis. This reflects the fact that RC stars are intermediate age stars (1-8 Gyr ago), so they have had sufficient time to diffuse throughout the SMC. The lack of RC stars ("hole") around (α = 18.8, δ = −73.25) is likely due to an extended cloud of obscuring matter (actually the "hole" is part of a large region showing large extinction - see Fig. 4 in Haschke, Grebel, & Duffau 2011). Indeed, when we look

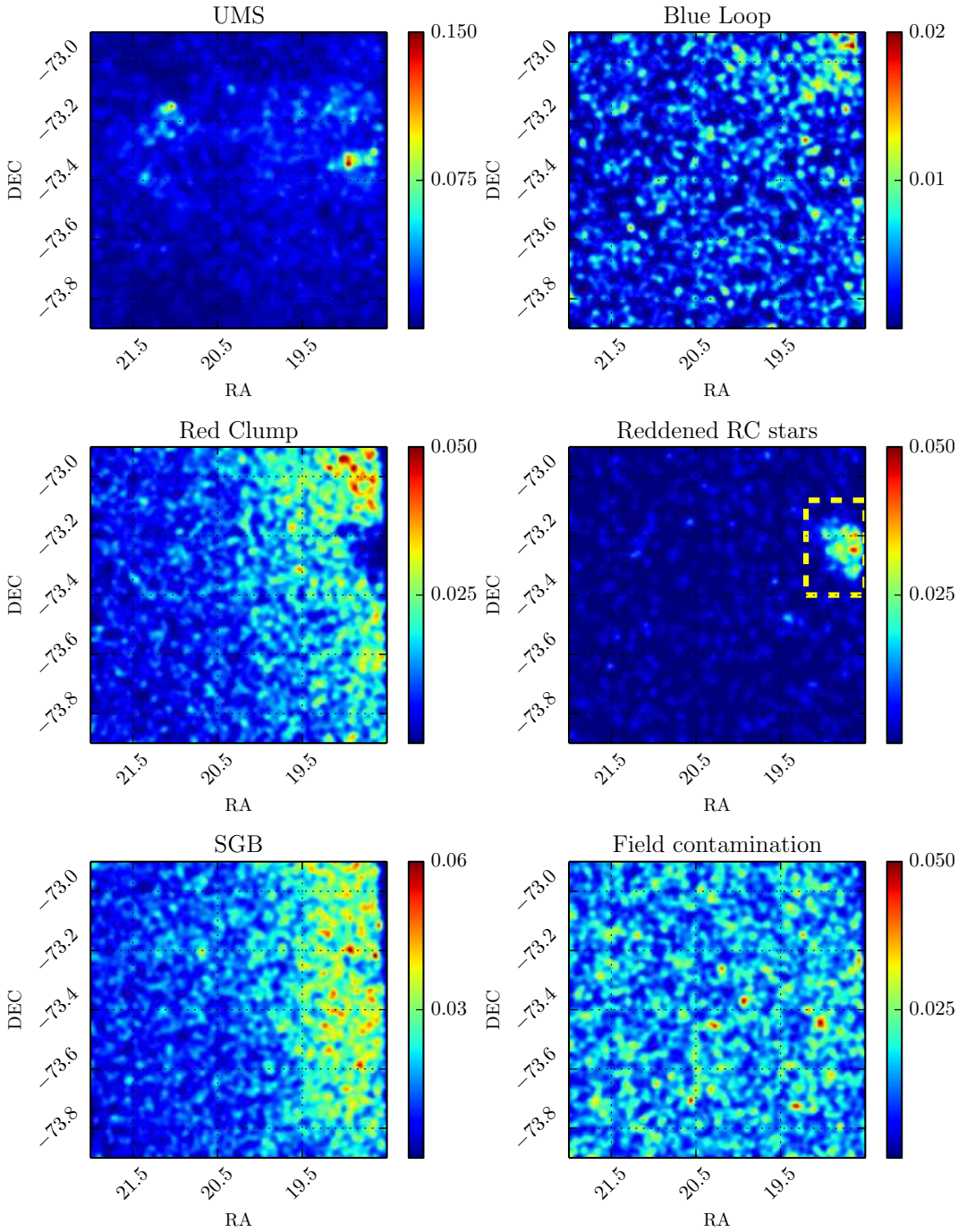

Figure 16. Tile 3_7. Spatial distributions of labeled CMD selections (see Fig. 15). Maps are produced by calculating a 2D histogram of stellar positions and then smoothing the result with a gaussian kernel. The yellow dashed box (in the middle-right panel) highlights a subregion where reddening is above the average (see Fig. 17).

at the map (middle-right panel) of stars taken from the yellow box in the CMD of Fig. 15 we find a clear overdensity at the location of the hole, hence suggesting that the missing RC stars are actually normal RC stars moved to the yellow box because of higher reddening. As a further support of this interpretation, Fig. 17 shows the CMD of all stars near the hole (yellow-dashed box in the middle-right panel of Fig. 16). Its elongated RC, broad RGB and upper MS are unique signatures of a large differential reddening. However, the total number of highly reddened stars is less than 1% of the stars in the entire tile, hence they are unnoticeable in the CMD of Fig. 12;

- The distribution of SGB stars (bottom-left panel) shows a net gradient of increasing concentration from left to right, without significant excess at the upper right corner (where BL stars are more concentrated). This mainly reflects the increasing number of star counts moving towards the SMC centre;
- Field contaminants (bottom right panel) are uniformly distributed over the FoV. The only few visible overdensities

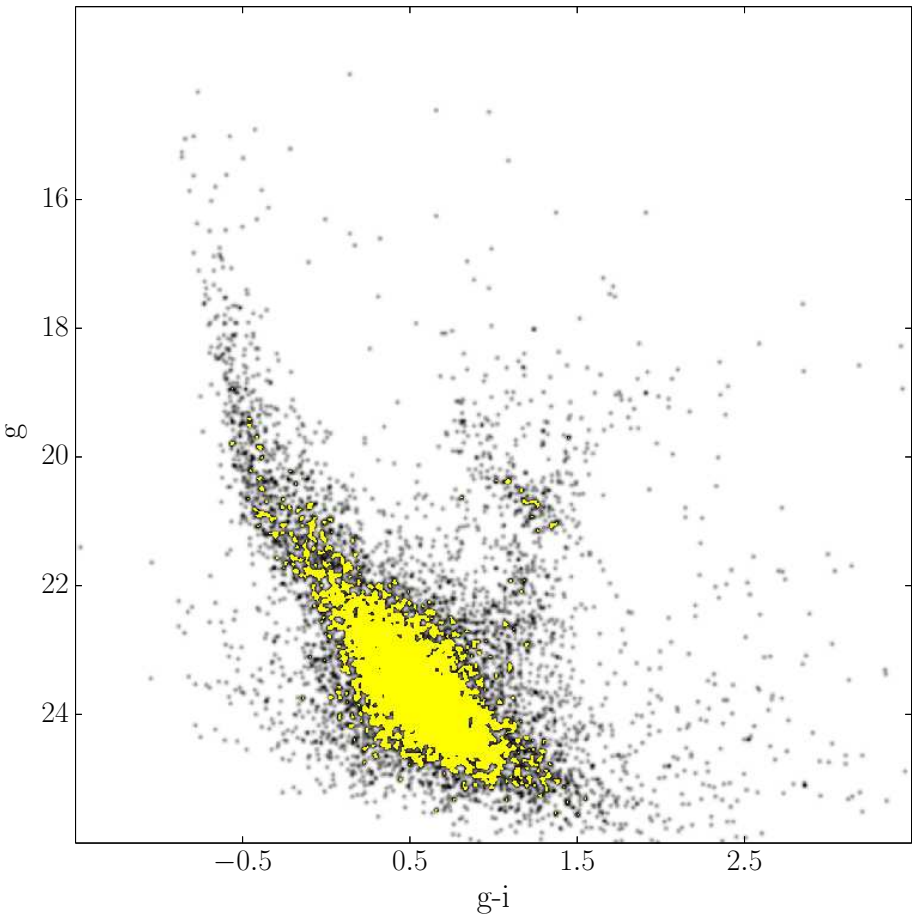

Figure 17. CMD for reddened stars in the tile 3_7 (yellow-dashed box in the middle-right panel of Figure 16.)

are likely due to MS stars scattered into the FC box because of the reddening.

4.2 Tile 4_6

4.2.1 CMD

Tile 4_6 hosts over four times more stars than tile 3_7. As a consequence crowding is more severe and the corresponding CMD (Figure 18) much shallower (but still one mag deeper than the oldest MSTO) and broader. In terms of stellar populations, there are two striking differences from 3_7's CMD (see Figure 12): 1) 4_6's CMD shows a prominent RGB bump, just above the RC, while this feature is missing in tile 3_7; 2) the morphology of the RC is rather elliptical in the 4_6 CMD, while it shows a clear protrusion towards brighter magnitudes in tile 3_7. In terms of age/metallicity the evidence of an RGB Bump brighter than the RC is a clear indication that intermediate and old star formation took place at relatively low metallicity (Z=0.001 or less) in tile 4_6. However, its apparent lack in the tile 3_7 CMD could be just due to the lower number of stars. On the other hand, the populous RC protrusion in the tile 3_7's CMD represents a significant difference from tile 4_6, since the latter is globally much more populated. Considering that the RC protrusion is likely populated by objects at the transition between RC and BL phases, therefore by stars with ages between 500 Myr and 1 Gyr, our conclusion is that tile 3_7 has been relatively more active than tile 4_6 at these epochs. If we take into account that tile 3_7 is in the Wing region, at the edge of the Bridge connecting the SMC to the LMC, it is tantalising to relate the enhanced star formation of tile 3_7 with an SMC/LMC interaction.

As for tile 3_7, the comparison with stellar isochrones shows an overall good agreement. We derive a reddening E(B-V)=0.04, which is lower than in tile 3_7. As in tile 3_7, the chosen isochrones do not bracket the whole colour distribution spread which characterises both the MS and RGB. In particular, the observational CMD extends much further to the red than the models, hence suggesting that a minor fraction of stars in tile 4_6 are either more reddened or more metal rich than the average of the tile. Once again, the division in sub-regions helps to disentangle the problem (see Fig. 19). Indeed, the sub-regions where the RGB is redder than models (for example, subregion F and I) are those whose MS is globally redder, which is more consistent with a reddening effect than a metallicity difference.

Concerning the MS, it is worth noticing that different subregions can show very different morphologies. For example, the CMD of subregion G shows a clear turn-off consistent with a star formation burst 100 or 200 Myr ago, while subregions like B show a much more extended MS, probably consistent with an activity extending to a few Myr ago. Interestingly, most of the regions show signs of the two events,

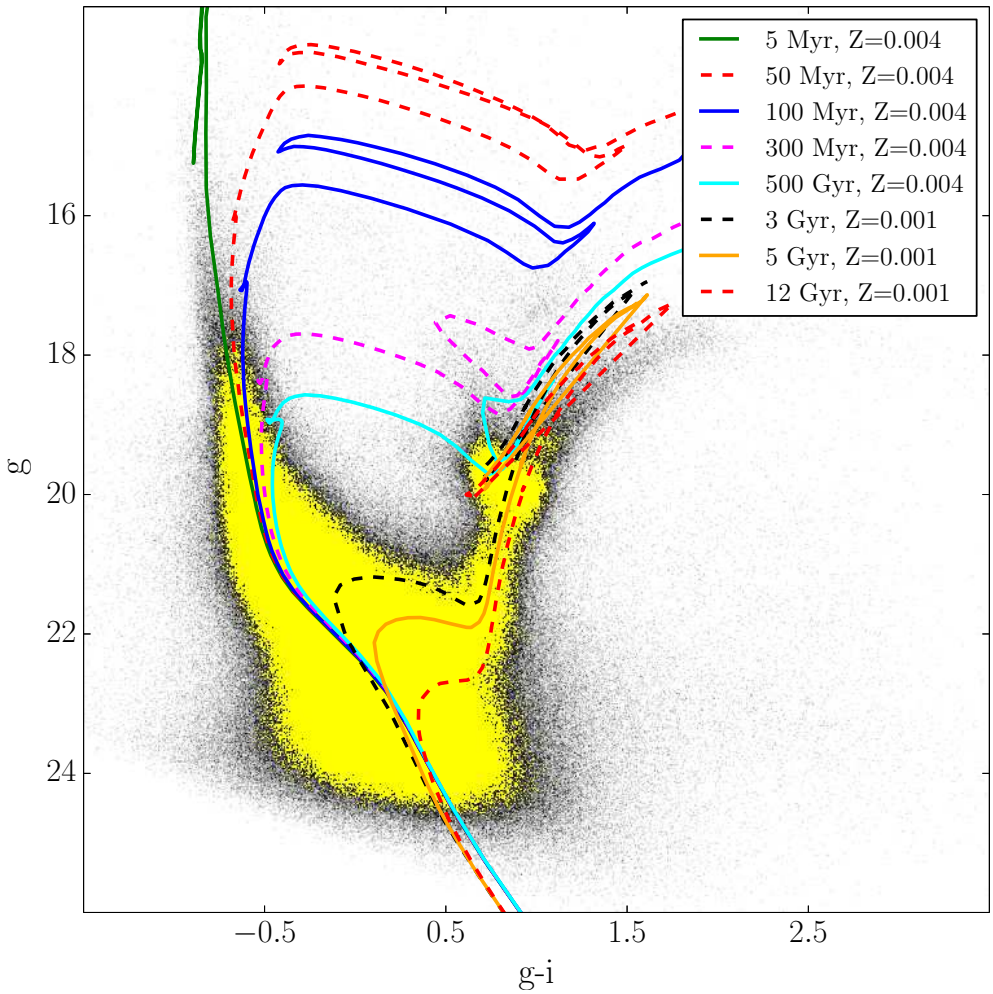

Figure 18. CMD of tile 4_6. The isochrone ages and metallicities are the same as in Figure 12. Assumed distance modulus and reddening E(B-V) are 18.9 mag and 0.04 mag, respectively.

suggesting that the star formation burst in one subregion could have triggered a burst in a neighbour subregion, as in the scenario derived by van Dyk, Puche, & Wong (1998) and Dohm-Palmer et al. (2002) for Sextans A.

4.2.2 Spatial distribution

Figure 20 shows how stars of different evolutionary phases are distributed over tile 4_6. Unlike tile 3_7, it is clear that 4_6 harbours many clusters and associations, probably because of the generally higher activity of the region. As in tile 3_7, the stellar density of older populations (RC and SGB, middle-left and bottom-left panels, respectively) increases smoothly towards the SMC centre (in this case, the lower right corner of tile 4_6), while the density of younger populations (UMS and BL, top-left and top-right panels, respectively) is very irregular and dominated by inhomogeneities. Indeed, most UMS stars are found aggregated in clusters/associations (identified clusters are indicated with labels c1 to c18 in the maps in Fig. 20; Table 9 shows their literature names and properties), with the most prominent ones corresponding to NGC 346 (c15 in the map) and NGC 371 (c9).

We point out that the distribution of RC stars shows clusters as well (c10, c11, c12), but none of them turns out to have a counterpart in the UMS map. A simple explanation is that all agglomerates found in the latter are younger than 100 Myr, hence too young to host RC stars[12]. Vice-versa, clusters detected only in the RC maps are necessarily too old to have UMS stars still alive. It is also worth of notice that among clusters visible using RC stars, namely c10, c11 and c12, only c10 and c12 are seen also in the SGB map. Indeed, the c11 cluster is the well known NGC 419 (see Table 9), which is about 1 Gyr old, hence the transition between the MS and the RGB phase, i.e. the SGB phase, is poorly populated (Hertzsprung Gap). Note the excellent correspondance between the literature ages reported in Table 9 and the evolutionary phase adopted to detect the different c1-c18 structures.

Finally, the map of reddened RC stars (middle-right panel) resembles that in tile 3_7 and suggests a very patchy reddening distribution.

[12] But old enough to host BL stars. Indeed, clusters c10 and c11 are clearly visible in the BL map.

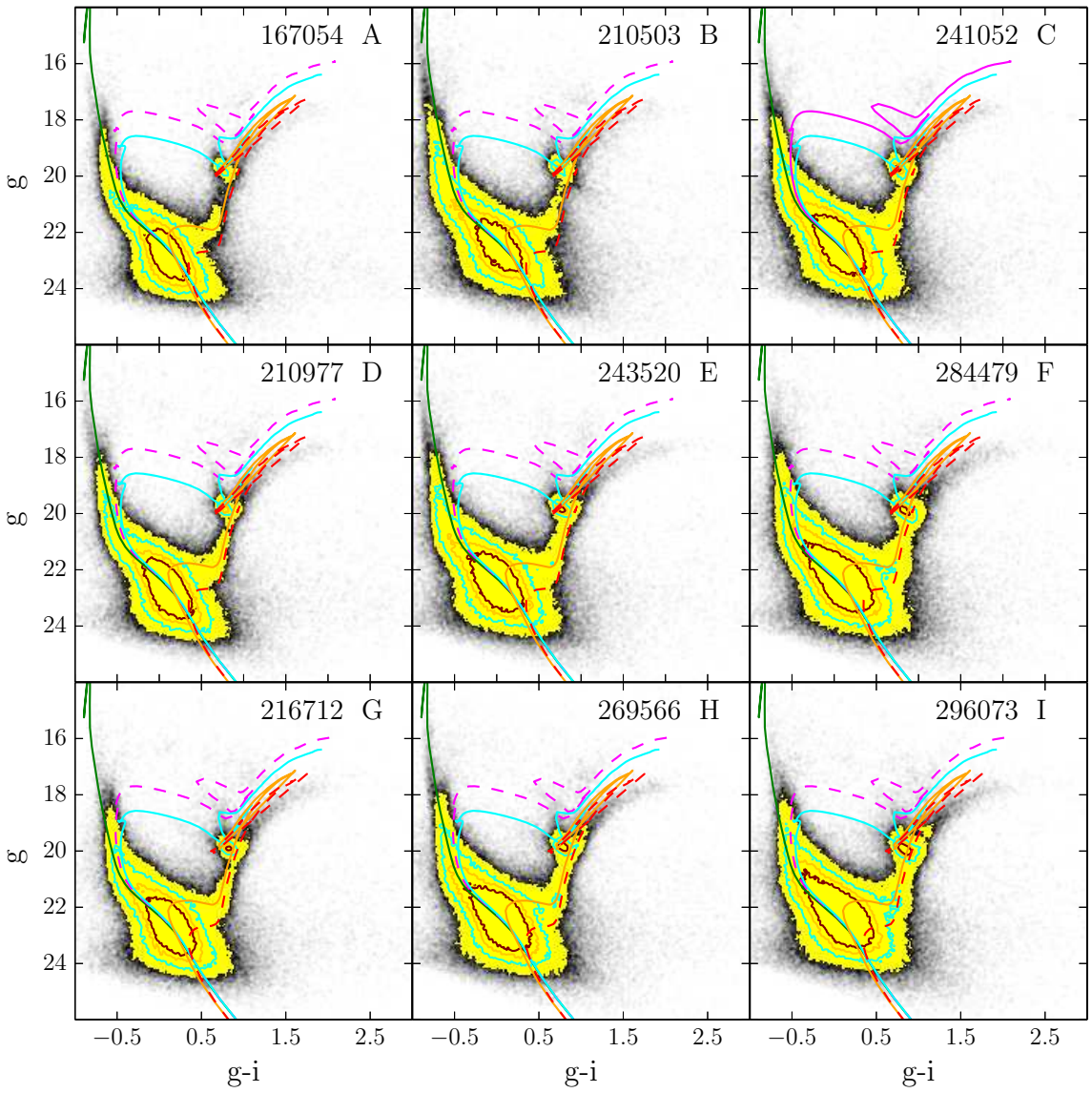

Figure 19. CMDs for nine $20' \times 21'$ arcmin subregions of tile 4_6. The isochrone ages and metallicities are the same as in Figure 12. Assumed distance modulus and reddening E(B-V) are 18.9 and 0.04, respectively.

5 STAR CLUSTERS IN STEP

As discussed in Sect. 2, the study of stellar clusters in the surveyed area is an important part of the STEP survey. In the previous section we have already discussed some of the clusters which can be readily identified in tile 4_6. The clusters (and associations) listed in Table 9 represent only part of the cluster/association content of tile 4_6. Indeed, the compilation by Bica et al. (2008) reports about 114 objects including both clusters and associations in tile 4_6 only. Clearly, most of these objects are small and a significant number of them could actually be asterisms. A detailed analysis of these objects is beyond the scope of present paper, and will be object of future works. Here, to give a flavour of the survey capabilities in such kind of studies, we present a more detailed analysis of two known clusters lying in tile 4_6, namely NGC 419 and IC 1624.

5.1 Surface brightness profiles of NGC 419 and IC 1624

The number density and surface brightness profiles (SBP) are useful tools to study the properties of star clusters in different galactic environments. These profiles contain information about the cluster's formation and evolution due to internal dynamic process and interaction with the galactic environment (see, e.g. Djorgovski & Meylan 1994; Gnedin & Ostriker 1997; Binney & Merrifield 1998; Lamers et al. 2005; Mackey & van den Bergh 2005, and references therein).

The most commonly used analytical functions to describe the SBPs of star clusters are those by King (1966) and by Elson, Fall & Freeman (1987); Elson (1999), i.e. the so called EFF profiles (similar to the Plummer 1915 model), being the latter particularly suited for young massive clusters in the MCs (see e.g. Elson 1999; Carvalho et al. 2008, and references therein). For this reason, in the following we

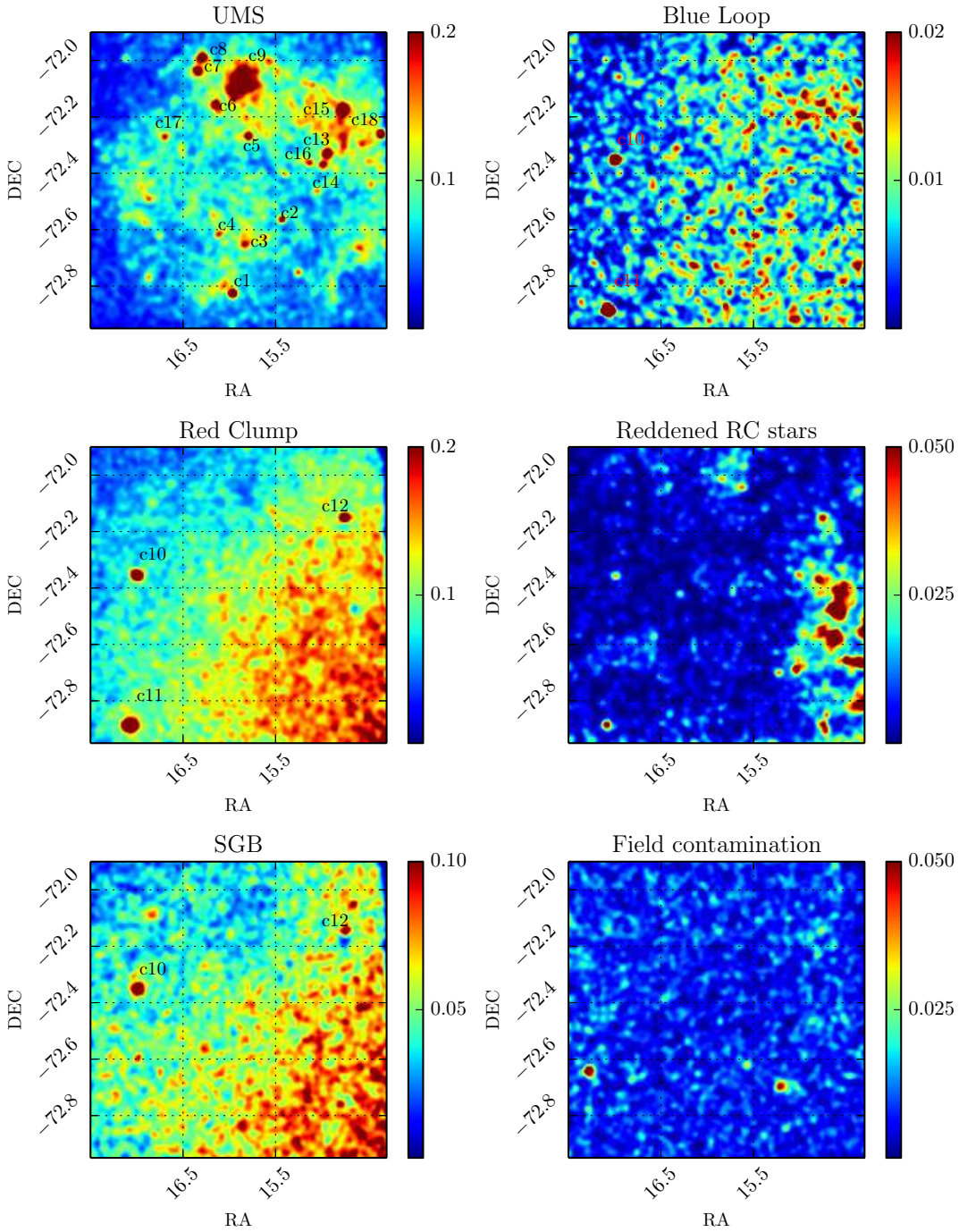

Figure 20. Tile 4_6. Spatial distributions of labeled CMD selections. Labels c1 to c18 indicate clusters identified by eye.

will adopt the EEF profiles to fit the SBPs of NGC 419 and IC 1624.

Given the high level of crowding in the cluster cores (with the consequent large incompleteness, especially in the case of NGC 419) we decided to avoid the use of the number density profile and to concentrate on the SBP. We followed the approach devised by e.g. Hill & Zaritsky (2006); Carvalho et al. (2008), consisting in building the profile shape to the integrated light, which does not suffer incompleteness.

To build the SBP for each cluster we followed closely the recipe by Carvalho et al. (2008), adopting also their coordinates for the cluster's centres. Details of the procedure can be found in section 2.2 of Carvalho et al. (2008). Here we recall that we measured the surface brightness in four sets of concentric annuli with radial steps of 1.5″, 2.0″, 3.0″, and 4.0″, centred on cluster's centres. We took the mean and the standard deviation of the counts in each annulus. The background was subtracted to the counts, after evaluating it in a number of loci in the surrounding of the clusters. The counts were eventually converted to magnitudes and plotted against the radius from the cluster centre. The result of such

Table 9. Cross-Identification of the over-densities found in Fig. 20. From left, the different columns show: the cluster ID of Fig. 20; the evolutionary phase in which they where identified; the equatorial coordinates; the SIMBAD name (L=Lindsay (1958); H86=Hodge (1986);BS=Bica & Schmitt (1995);B=Brueck (1976)); the classification (NA=Nebula-Association; C=Cluster; A=Association), the major and minor axis according to Bica et al. (2008); the age and the reference for the age estimate: a) Chiosi et al. (2006); b) Glatt et al. (2010); c) Rochau et al. (2007); d) Glatt et al. (2008b).

ID	Ev. Phase	RA (J2000) deg	DEC (J2000) deg	Name	Class.	Major Axis arcmin	Minor Axis arcmin	log(Age) Gyr	Age Ref.
c1	UMS	15.9708	-72.8261	NGC 376	C	1.8	1.8	7.50	b
c2	UMS	15.4375	-72.5644	L66	C	1.1	1.1	7.40	b
c3	UMS	15.8458	-72.6517	B115	C	0.9	0.8	7.60	b
c4	UMS	16.0583	-72.6469	BS118	A	1.3	0.9	6.9	a
c5	UMS	15.8	-72.2725	L70	C	0.75	0.75	7.60	b
c6	UMS	16.15	-72.1606	L74	C	1.0	1.0	7.00	b
c7	UMS	16.3417	-72.0431	IC 1624	C	0.9	0.9	8.35	b
c8	UMS	16.2792	-71.9936	NGC 395	NA	1.1	1.1	7.2	a
c9	UMS	15.8708	-72.0567	NGC 371	NA	4.2	3.8	6.7	a
c10	BL,RC,SGB	16.9958	-72.3556	NGC 416	C	1.7	1.7	9.80	d
c11	BL,RC	17.0792	-72.8842	NGC 419	C	2.8	2.8	9.00	d
c12	RC,SGB	14.775	-72.1508	BS90	C	1.0	1.0	9.6	c
c13	UMS	14.95	-72.3339	IC 1611	C	1.5	1.5	8.20	b
c14	UMS	14.9875	-72.3733	H86-186	C	0.6	0.6	8.20	b
c15	UMS	14.7708	-72.1769	NGC 346	NA	8.5	8.5	7.2	a
c16	UMS	15.1417	-72.3656	L63	C	0.85	0.85	7.80	b
c17	UMS	16.7	-72.2736	L79	C	0.9	0.9	7.55	b
c18	UMS	14.3792	-72.2644	L56	C	0.95	0.95	7.80	b

a procedure is shown in the upper-right panel of Figures 21 and 22 for NGC 419 and IC 1624, respectively.

We then employed the EFF model to analyse the SBPs of the target clusters. Its analytical formulation in magnitudes is:

$$\mu(r) = \mu(0) + 1.25\gamma \log(1 + r^2/\alpha^2) \qquad (2)$$

where $\mu(0)$ is the central surface brightness in magnitudes, α is a measure of the core radius[13] and γ is the power-law slope. The parameter α in the EFF profiles is related to the core radius of a cluster by $r_c = \alpha \cdot (2^{2/\gamma} - 1)^{1/2}$. Equation 2 is equal to the original Plummer (1915) function for γ=4, whereas an empirically derived value suited for the (young) MC cluster is 2.7 (Elson, Fall & Freeman 1987; Carvalho et al. 2008).

We adopted a weighted least-square method to fit Eq. 2 to the observed SBPs. In order to obtain a better profile, we restricted the fit to a maximum radius (fitting radius) beyond which the cluster is no longer distinguishable from the background. We adopt this fitting radius in the next section as a limit to decide whether or not a star belongs to the cluster. The fitting radius is shown as a dashed line in the upper-right panel of Figures 21 and 22. In the same figures, a solid red line shows the result of the fit, while Tab. 10 lists the values of the relevant parameters of Eq. 2.

[13] According to the original Plummer (1915) paper, "The α parameter may be regarded as the radius of the equivalent homogeneous or uniform cluster, containing the same number of stars and having the same volume density, or the same areal density, as the actual cluster at its centre."

Table 10. Results of the stellar density profile fit obtained with Eq. 2.

Cluster	$\mu_g(0)$ mag arcsec^{-2}	α arcsec	γ	Fit. radius arcsec
NGC 419	18.18±0.01	14.8±0.3	2.52±0.03	85
IC 1624	19.11±0.04	15.0±1.5	3.2±0.3	39

These values compare well with similar analyses present in the literature. In particular, for cluster NGC 419, our results appear to be in good agreement with those by Hill & Zaritsky (2006); Carvalho et al. (2008); Glatt et al. (2009), taking also into account the difference in the adopted filter (g instead of V), centre coordinates (apart Carvalho et al. 2008), spatial resolution (ccd pixel size), extension (size of the frame) and depth of the exposures used in these different investigations. As for IC 1624, the agreement with Carvalho et al. (2008) is worse, (especially for $\mu(0)$); this is perhaps due to the different statistics adopted (see Sec. 2.2 and Tab. 3 in Carvalho et al. 2008).

5.2 The age of NGC 419 and IC 1624

As mentioned in the previous section, we assumed the fitting radius to be a (rough) measure of the "effective" cluster radius (i.e. we consider all stars within this radius as belonging to the cluster). The soundness of our choice is confirmed by looking at the upper-left panels of Figures 21 and 22, even if

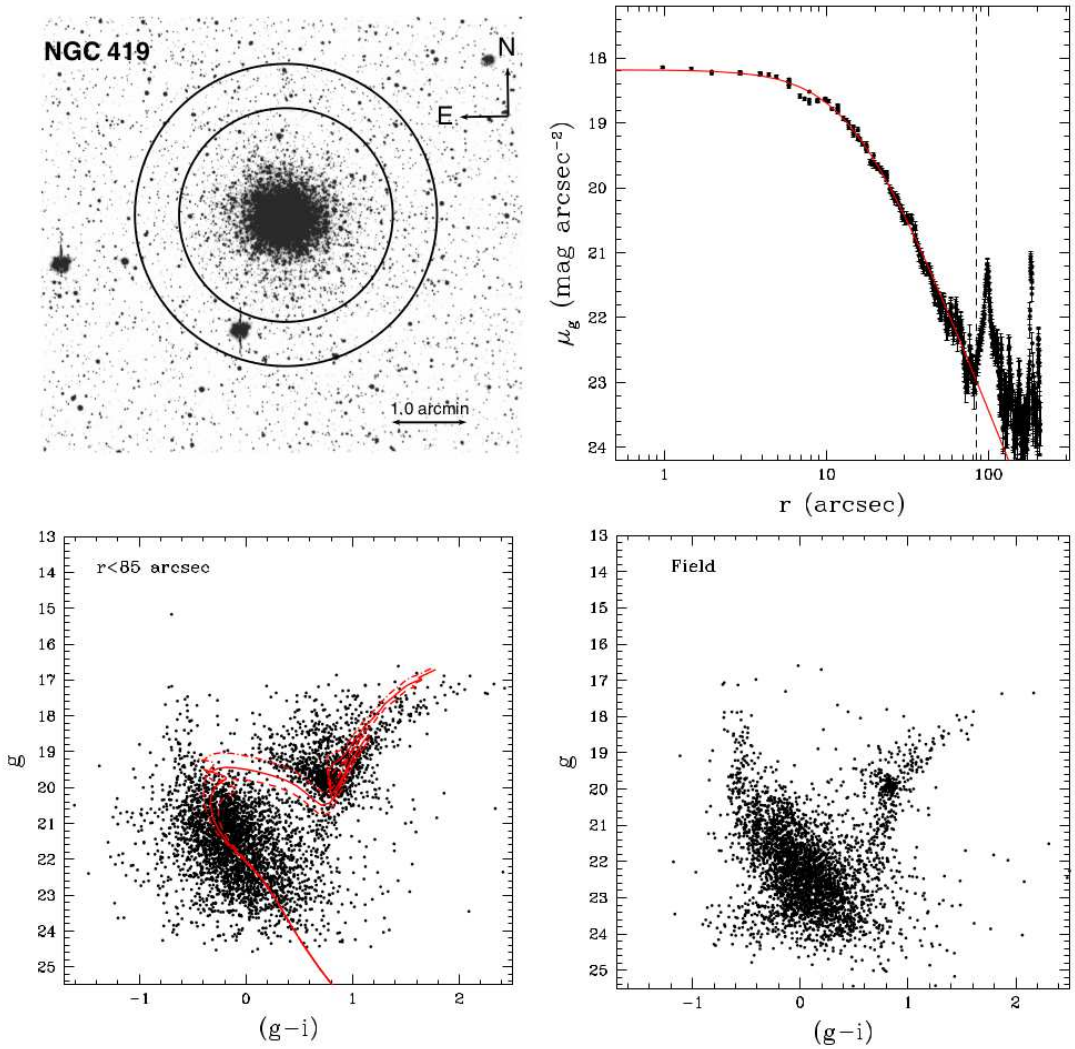

Figure 21. Upper-left panel: cluster map; the two circles have radii of 85″ and 120″, respectively. Upper-right panel: black dots show the observed radial stellar surface brightness profile around the NGC 419 center. The solid red line shows the profile fitting obtained with eq. 2, while the dashed line represents the fitting radius (see text). Lower-left panel: CMD of the cluster within the fitting radius (see text). Lower-right panel: field stars in an annulus with inner and outer radii of 85″ and 120″, respectively. This annulus has the same area as the innermost circle.

some contamination from the field is still present (see lower-panels of Fig. 22). Furthermore, the fitting radii estimated here agree very well with (half of) the major and minor axes (according to Bica et al. 2008) listed in Tab. 9 for the two clusters.

The CMDs of NGC 419 and IC 1624, as well as those of the surrounding fields are shown in the lower-left and lower-right panels of Figures 21 and 22, respectively. The CMD of NGC 419 is rather scattered, due to the high crowding, which boosts dramatically photometric errors and incompleteness towards the cluster centre. Indeed, the CMD within the effective radius is almost 1 mag shallower than the CMD of the external field. On the other hand, the CMD of IC 1624 is rather loose because of the global paucity of stars in this cluster.

In terms of age, there is a clear difference between the two clusters, with IC 1624 being much younger than NGC 419 (see also Tab. 9). To be more quantitative, we adopted the isochrones by Marigo et al. (2008) to estimate the ages of the two clusters. The best-fitting models are shown in Figures 21 and 22 (lower-left panels) whereas the age and the other relevant parameters are listed in Table 11 (we recall here that the calibration, especially for blue colours is subject to improvement, which can affect e.g. the reddening estimate in Table 11).

NGC 419 is known to host multiple stellar populations. A visual inspection of higher resolution data (HST/HRC, see Fig. 42 in Glatt et al. 2008a) shows clearly a very broad MSTO, more consistent with a prolonged SF than a single burst population. Indeed, using isochrone fitting applied to MSTO stars, Glatt et al. (2008a) found an age spread between 1.2 and 1.6 Gyr. Afterwards, Girardi et al. (2009) reanalysed the data modelling the CMD with synthetic populations, and concluded that only an age spread of about Δ logage$\approx$ 0.15 dex allows to reproduce the MSTO and RC morphologies simultaneously. In our data, the magnitude

Table 11. Results from the isochrone fitting procedure for NGC 419 and IC 1624 (see text).

Cluster	$(m-M)_0$ mag	$E(B-V)$ mag	Z	Age Myr
NGC 419	18.80	0.04	0.004	700,900,1100
IC 1624	19.0	0.02	0.004	170

difference between RC and bulk of the MSTO suggests an age between 900 and 1100 Myr (see the bottom-left panel in Fig. 21), but the large photometric errors prevent any definitive conclusion about a genuine age spread. In this regard, it is also worth of notice the large number of stars just above the RC, which are not seen in the external field. The presence of these object can be naturally explained in terms of blending due to the severe crowding conditions. Anyway, we cannot exclude that the innermost region of the cluster is harbouring an even younger sub-population (composed by BL stars).

The situation is completely different in IC 1624. The 170 Myr old isochrone (see Fig. 22) fits very well all the main evolutionary phases, including the MSTO (around $g \sim 18$ mag), the red envelope of the BL ($g-i \sim 0.8$ mag) and the average luminosity of the loop. Interestingly, the field around the cluster appears to be younger than the cluster itself. This is not surprising given the proximity of the young Nebula-Association NGC 395 (see Figures 6, 20 and Table 9).

6 SUMMARY

The STEP survey is a deep, homogeneous and uniform g, r, i, H_α survey of $\sim$72 deg^2 across the SMC and the Bridge, as well as 2 deg^2 on the Magellanic Strem. The STEP observations, based on INAF VST Guaranteed Time Observations, started on November 2011.

The STEP data will provide, among other things, a detailed history of star formation across the SMC and the Bridge, and an inventory of variable stars along eight fields in the Bridge, outside the region investigated by the OGLE III survey.

This paper presents the STEP survey strategy, the technique adopted for the data reduction and the first results aimed at assessing their scientific quality.

The data presented here show the potential of the survey in addressing its main science goals and validate the adopted observing strategy. In particular, we analysed qualitatively two tiles, namely tiles 4_6 and 3_7, centred on the north of the SMC bar and on the Wing, respectively. The CMDs of these fields show a wealth of substructures and a clear separation between the various populations hosted in the galaxy. It is also clear that our photometry allows us to investigate in detail the populations producing the oldest MSTO in the galaxy, i.e. one of the main aim of this survey. These diagrams will form the base of the SFH analysis which will be the subject of future papers.

To illustrate some additional scientific applications of the STEP survey, we investigated two stellar clusters falling into the 4_6 tile, namely NGC 419 and IC 1624. We used the stellar radial density profiles to estimate their structural parameters, whereas the analysis of their CMDs allowed us to estimate their age by means of isochrone-fitting.

Finally, the STEP survey will be of great importance for the astronomical community because it represents the optical complement to the VMC ESO public survey (Cioni et al. 2011) which is surveying the Magellanic System in the near infrared YJK_s bands at a comparable level of sensitivity. Similarly, STEP will complement the HST observations already obtained in the optical bands, that, albeit immeasurably better for resolution and depth, are nevertheless confined to small FoVs throughout the SMC. Finally, we plan to release to the community the catalogues as well as the reduced images as soon as they are fully validated.

ACKNOWLEDGMENTS

We wish to thank our anonymous Referee for his/her competent and useful review that helped us to improve the paper.

Partial support to this work was provided by the following projects: PRIN-MIUR 2010 (2010LY5N2T) "Chemical and Dynamical evolution of the Milky Way and Local Group galaxies" (PI F. Matteucci); PRIN-INAF 2011 "Galaxy evolution with the VLT Surveys Telescope (VST)" (PI A. Grado); PRIN-INAF 2011 "Tracing the formation and evolution of the Galactic halo with VST" (PI M. Marconi).

We acknowledge Amata Mercurio and Crescenzo Tortora for helpful discussions about the CMD contamination caused by faint extragalactic sources.

We thank the VST Center for providing access to its computational infrastructures.

This research has made use of the SIMBAD database and VizieR catalogue access tool, operated at CDS, Strasbourg, France

Funding for SDSS-III has been provided by the Alfred P. Sloan Foundation, the Participating Institutions, the National Science Foundation, and the U.S. Department of Energy Office of Science. The SDSS-III web site is http://www.sdss3.org/. SDSS-III is managed by the Astrophysical Research Consortium for the Participating Institutions of the SDSS-III Collaboration including the University of Arizona, the Brazilian Participation Group, Brookhaven National Laboratory, University of Cambridge, Carnegie Mellon University, University of Florida, the French Participation Group, the German Participation Group, Harvard University, the Instituto de Astrofisica de Canarias, the Michigan State/Notre Dame/JINA Participation Group, Johns Hopkins University, Lawrence Berkeley National Laboratory, Max Planck Institute for Astrophysics, Max Planck Institute for Extraterrestrial Physics, New Mexico State University, New York University, Ohio State University, Pennsylvania State University, University of Portsmouth, Princeton University, the Spanish Participation Group, University of Tokyo, University of Utah, Vanderbilt University, University of Virginia, University of Washington, and Yale University.

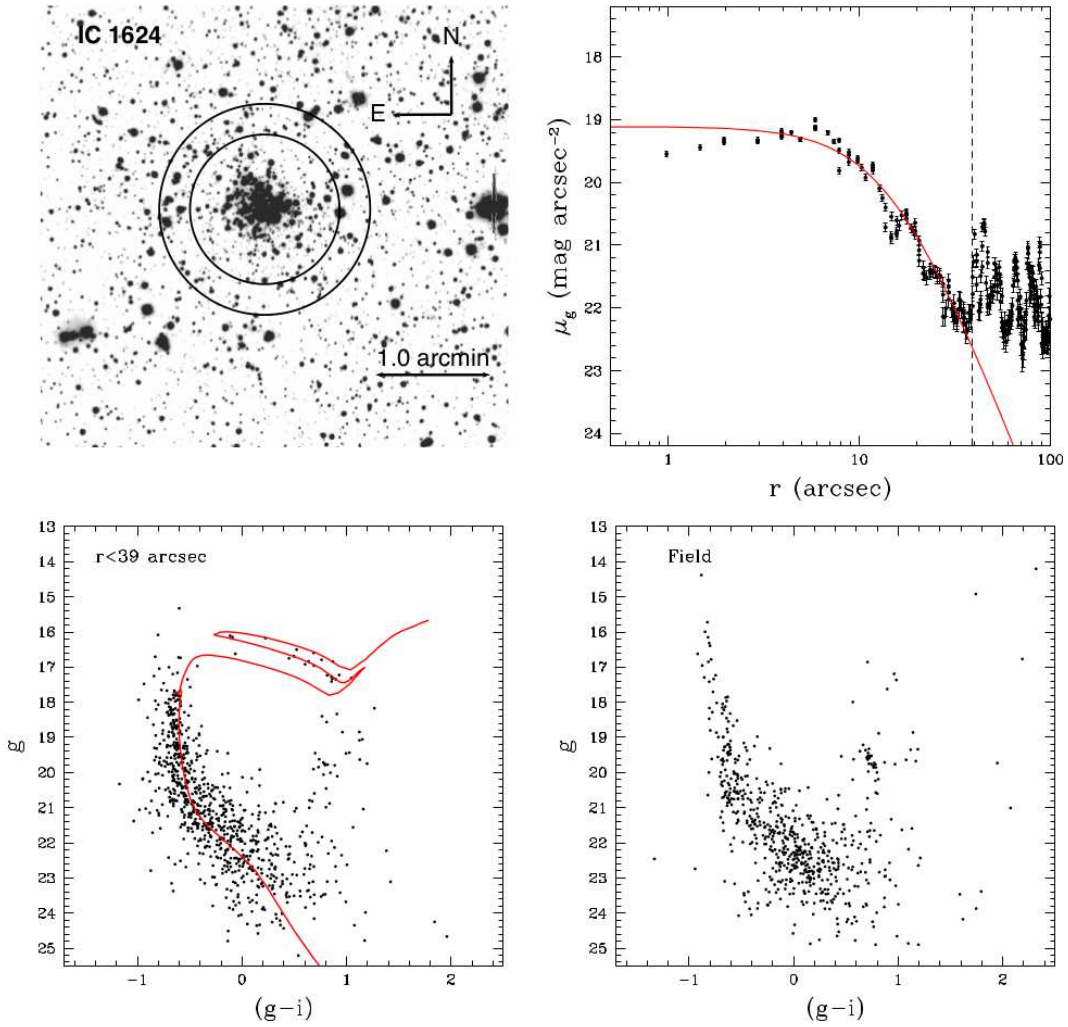

Figure 22. Same as in Fig. 21, but for cluster IC 1624. In this case inner and outer circles have radii of 39″ and 55″, respectively.

REFERENCES

Andersen, M. I.; Freyhammer, L.; Storm, J. 1995, ESO Conference, 53, 87

Arnaboldi, M., Dietrich, J., Hatziminaoglou, E., et al., 2008, The Messenger, 134, 42

Bagheri, G. et al. 2013, A&A, 551, A78

Bekki K., Chiba M., 2007, MNRAS, 381, L16

Bekki K., Stanimirović S., 2009, MNRAS, 395, 342

Bertin E. et al. 2002, ASP Conference Series, 281, 228

Bertin E., 2006, ASP Conference Series, 351, 112

Bica, E. L. D., & Schmitt, H. R. 1995, ApJS, 101, 41

Bica, E., Bonatto, C., Dutra, C.M., Santos, J.F.C., 2008, MNRAS, 389, 678

Binney J., Merrifield M., 1998, in Galactic Astronomy (Princeton, NJ: Princeton University Press), Princeton series in Astrophysics

Bothun, G.D., Thompson, I.B., 1988, AJ, 96, 877

Bouret J.-C., Lanz T., Martins F., Marcolino W. L. F., Hillier D. J., Depagne E., Hubeny I., 2013, A&A, 555, A1

Brueck, M. T. 1976, Occasional Reports of the Royal Observatory Edinburgh, 1,

Brüns C., et al., 2005, A&A, 432, 45

Butler D., Demarque P., Smith H. A., 1982, ApJ, 257, 592

Capaccioli M. & Schipani P. 2011, The Messenger, 146, 2

Carlson, L. R., Sabbi, E., Sirianni, M., et al.P 2007, ApJ, 665, L109

Carvalho, L., Saurin, T. A., Bica, E., Bonatto, C., & Schmidt, A. A. 2008, A&A, 485, 71

Castellani, V., Cignoni, M., Degl'Innocenti, S., Petroni, S., & Prada Moroni, P. G. 2002, MNRAS, 334, 69

Chiosi, E., Vallenari, A., Held, E.V., Rizzi, L., Moretti, A. 2006, A&A, 452, 179

Cignoni, M., Ripepi, V., Marconi, M., et al. 2007, A&A, 463, 975

Cignoni, M, Tosi, M.2010, in Dwarf Galaxies and Cosmology, Advances in Astronomy (Hindawi), vol. 3

Cignoni, M., Tosi, M., Sabbi, E., et al. 2010, ApJl, 712, L63

Cignoni, M., Tosi, M., Sabbi, E., Nota, A., & Gallagher, J. S. 2011, AJ, 141, 31

Cignoni, M., Cole, A.A., Tosi, M., Gallagher, J. S., Sabbi, E., Anderson, J, Grebel, E.K., Nota, A., & 2012, ApJ, 754,130

Cignoni, M., Cole, A. A., Tosi, M., et al. 2013, ApJ, 775,

83
Cioni, M.-R. L., Clementini, G., Girardi, L., et al. 2011, A&A, 527, A116
Cooper A. P., et al., 2010, MNRAS, 406, 744
de Vaucouleurs G., de Vaucouleurs A., Corwin H. G., Jr., Buta R. J., Paturel G., Fouqué P., 1991, Third Reference Catalogue of Bright Galaxies. Vol. 1-3 (Berlin: Springer), 2069 pp, chap XII
De Lucia G., Helmi A., 2008, MNRAS, 391, 14
Djorgovski S., Meylan G., 1994, AJ, 108, 1292
Dolphin, A.E., Walker, A.R., Hodge, P.W., Mateo, M., Olszewski, E.W., Scommer, R.A., & Suntzeff, N.B. 2001, ApJ, 562, 303
Dohm-Palmer, R. C., Skillman, E. D., Mateo, M., et al. 2002, AJ, 123, 813
Elson R. A. W., Fall S. M., & Freeman K. C. 1987, ApJ, 323, 54
Elson R. A. W., 1999, in "Globular Cluster, 10th Canary Islands Winter School of Astrophysics", Cambridge University Press, p. 209
Fukugita M., Ichikawa T., Gunn J. E., Doi M., Shimasaku K., Schneider D. P., 1996, AJ, 111, 1748
Girardi, L., Rubele, S., & Kerber, L. 2009, MNRAS, 394, L74
Glatt, K., Gallagher, J. S., III, Grebel, E. K., et al. 2008a, AJ, 135, 1106
Glatt, K., Grebel, E. K., Sabbi, E., et al. 2008b, AJ, 136, 1703
Glatt, K. et al. 2009, AJ, 138, 1403
Glatt, K., Grebel, E. K., & Koch, A. 2010, A&A, 517, A50
Glatt, K., Grebel, E. K., Jordi, K., et al. 2011, AJ, 142, 36
Gnedin O. Y., Ostriker J. P., 1997, ApJ, 474, 223
Gonzalez G., Wallerstein G., 1998, AJ, 116, 765
Grado A., Capaccioli M., Limatola L., Getman F. 2012, MemSait, 19, 362
Gunn J. E., Hogg D., Finkbeiner D., Schlegel D., 2001, http://www.sdss.org/dr7/algorithms/jeg_photometric_eq_dr1.html#usno2SDSS
Harries, T. J., Hilditch, R. W., & Howarth, I. D. 2003, MNRAS, 339, 157
Harris, J., & Zaritsky, D. 2004, AJ, 127, 1531
Harris, 2007, ApJ, 658, 345
Haschke R., Grebel E. K., Duffau S., 2011, AJ, 141, 158
Haschke R., Grebel E. K., Duffau S., 2012, AJ, 144, 107
Haschke R., Grebel E. K., Frebel A., Duffau S., Hansen C. J., Koch A., 2012, AJ, 144, 88
Hatzidimitriou, D., & Hawkins, M. R. S. 1989, MNRAS, 241, 667
Hatzidimitriou, D., Stanimirović, S., Maragoudaki, F., et al., 2005, MNRAS, 360, 117
Hill A., Zaritsky D., 2006, AJ, 131, 414
Hindman J. V., Kerr F. J., McGee R. X., 1963, AuJPh, 16, 570
Hodge, P. 1986, PASP, 98, 1113
Hunter I., et al., 2007, A&A, 466, 277
Hunter I., et al., 2009, A&A, 496, 841
Irwin M. J., Kunkel W. E., Demers S., 1985, Natur, 318, 160
Irwin, M., 1991, IAUS, 148, 453
Ivezić, Ž. et al. 2007, AJ, 134, 973
Jordi K., Grebel E. K., Ammon K., 2006, A&A, 460, 339
Kallivayalil, N., van der Marel, R. P., & Alcock, C. 2006, ApJ, 652, 1213
Kallivayalil et al. 2013, ApJ, 764, 161
Kayser A., Hilker M., Grebel E. K., Willemsen P. G., 2008, A&A, 486, 437
Keller S. C., et al., 2007, PASA, 24, 1
King I. R., 1966, AJ, 71, 64
Kuijken K. 2011, The Messenger, 146, 8
Kunth D., Östlin G., 2000, A&ARv, 10, 1
Kurt C. M., Dufour R. J., 1998, RMxAC, 7, 202
Lamers H. J. G. L. M., Gieles M., Bastian N., Baumgardt H., Kharchenko N. V., Portegies Zwart S., 2005, A&A, 441, 117
Lindsay, E. M. 1958, MNRAS, 118, 172
Mackey A. D., van den Bergh S., 2005, MNRAS, 360, 631
Marigo, P., Girardi, L., Bressan, A., et al. 2008, A&A, 482, 883
McCumber, M.P., Garnett, D.R., Dufour, R.J. 2005, AJ, 130, 1083
Muller, E., Staveley-Smith, L., Zealey, W., Stanimirović, S., 2003, MNRAS, 339, 105
Noël, N.E.D., Gallart, C., Costa, E., & Méndez, R.A. 2007, AJ, 133, 2037
Noël, N. E. D., Aparicio, A., Gallart, C., et al. 2009, ApJ, 705, 1260
Noël et al. 2013, arXiv:1303.3014
Nota, A., Sirianni, M., Sabbi, E., et al. 2006, ApJl, 640, L29
Olsen K. A., et al., 2014, AAS, 223, #254.44
Plummer H.C. 1915, MNRAS, 76, 107
Robotham et al. 2012, MNRAS, 424, 1448
Rochau, B., Gouliermis, D. A., Brandner, W., Dolphin, A. E., & Henning, T. 2007, ApJ, 664, 322
Rubele, S., Kerber, L., Girardi, L., et al. 2012, A&A, 537, A106
Russell, S. C., & Bessell, M. S. 1989, ApJS, 70, 865
Sabbi, E., Sirianni, M., Nota, A.,Tosi, M., Gallagher, J.S., Meixner, M.;,Oey, M. S., Walterbos, R., et al. 2007, AJ, 133, 44
Sabbi, E., Gallagher, J.S., Tosi, M., , Anderson, J., Nota, A., Grebel, E.K., Cignoni, M., Cole, A.A. et al . 2009, ApJ, 703, 721
Saha A., et al., 2010, AJ, 140, 1719
Schipani P., et al., 2012, JOSAA, 29, 1359
Sewiło M., et al., 2013, ApJ, 778, 15
Shapley H., 1940, BHarO, 914, 8
Shara M. M., Fall S. M., Rich R. M., Zurek D., 1998, ApJ, 508, 570
Smith J.A., Tucker D.L., Kent S., et al. 2002, AJ, 123, 2121
Staveley-Smith, L., Kim, S., Calabretta, M.R., et al., 2003, MNRAS, 339, 87
Stetson, P. B. 1987, PASP, 99, 191
Stetson, P. B. 1992, Astronomical Data Analysis Software and Systems I, 25, 297
Subramanian, S., & Subramaniam, A. 2009, A&A, 496, 399
Subramanian S., Subramaniam A., 2012, ApJ, 744, 128
Tolstoy, E., Hill, V., Tosi, M. 2009, ARAA 47, 371
Tosi, M., Greggio, L., Marconi, G., & Focardi, P. 1991, AJ, 102, 951
Tosi, M., Sabbi, E., Bellazzini, M., et al. 2001, AJ, 122, 1271
Udalski A., Szymanski M., Kubiak M., Pietrzynski G., Soszynski I., Wozniak P., Zebrun K., 1999, AcA, 49, 201

Udalski A., et al., 2008, AcA, 58, 329
Vandenberg, D. A., & Bell, R. A. 1985, ApJS, 58, 561
van Dyk S. D., Puche D., Wong T., 1998, AJ, 116, 2341
Weisz D. R., Dolphin A. E., Skillman E. D., Holtzman J., Dalcanton J. J., Cole A. A., Neary K., 2013, MNRAS, 431, 364
Zaritsky D., Harris J., Grebel E. K., Thompson I. B., 2000, ApJ, 534, L53
Zaritsky D., Harris J., Thompson I. B., Grebel E. K., Massey P., 2002, AJ, 123, 855